

Benthic foraminiferal turnover across the Dan-C2 event in the eastern South Atlantic Ocean (ODP Site 1262)

Gabriela J. Arreguín-Rodríguez^{a,b,c*}, James S. K. Barnett^{d,e}, Melanie J. Leng^{f,g}, Kate Littler^d, Dick Kroon^h, Daniela Schmidtⁱ, Ellen Thomas^{j,k}, and Laia Alegret^{a,l}

^a Departamento de Ciencias de la Tierra, Universidad de Zaragoza, Pedro Cerbuna 12, 50009, Zaragoza, Spain

^b Centro Interdisciplinario de Ciencias Marinas, Instituto Politecnico Nacional, La Paz, Mexico

^c Facultad de Ciencias Marinas, Universidad Autonoma de Baja California, Ensenada, Mexico

^d Camborne School of Mines, and Environment and Sustainability Institute, Penryn Campus, University of Exeter, TR10 9FE, UK

^e School of Earth and Environmental Sciences, University of St Andrews, St Andrews, Scotland, KY16 9AL, UK

^f British Geological Survey, Keyworth, Nottingham NG12 5GG, UK

^g School of Biosciences, University of Nottingham, Loughborough LE12 5RD, UK

^h School of GeoSciences, University of Edinburgh, West Mains Road, Edinburgh EH9 3JW, UK

ⁱ School of Earth Sciences, University of Bristol, BS8 1RJ Bristol, UK

^j Department of Earth and Planetary Sciences, Yale University, New Haven, Connecticut, USA

^k Department of Earth and Environmental Sciences, Wesleyan University, Middletown, Connecticut, USA

^l Instituto Universitario de Ciencias Ambientales, Universidad de Zaragoza, Zaragoza, Spain

*Corresponding author: arreguing@uabc.edu.mx

Abstract

The Paleogene was punctuated by perturbations of the global carbon cycle, many associated with transient global warming events (hyperthermals). The Dan-C2 event (~160 kyr after Cretaceous/Paleogene boundary; K/Pg) was the oldest of these eccentricity-linked carbon cycle disturbances (ELCD). In contrast to other hyperthermals, the Dan-C2 event was not characterised by bottom water warming, and surface water warming probably was not global. Benthic foraminiferal assemblages across Dan-C2 at SE Atlantic Ocean Drilling Program (ODP) Site 1262 are diverse and strongly dominated by calcareous species.

Epifaunal and infaunal morphogroups are equally abundant, suggesting meso-oligotrophic seafloor conditions. Assemblages decreased in diversity gradually before Dan-C2, and *Nuttallides truempyi* decreased in relative abundance while *Stensioeina beccariiiformis* and the agglutinant *Spiroplectammina spectabilis* increased, suggesting enhanced food supply to the seafloor. Benthic foraminifera were not highly affected by the Dan-C2 event. An increase in relative abundance of the opportunistic species *Bulimina kugleri* and *Seabrookia cretacea* after Dan-C2 points to a change in the type of organic matter arriving at the seafloor. These changes may have been caused by ongoing environmental and/or evolutionary instability following K/Pg mass extinction of oceanic plankton. Variability in composition of pelagic ecosystems, thus the type and/or amount of food arriving at the seafloor, may have been caused by the gradual recovery of pelagic ecosystems after that extinction, possibly affected by warming and pH changes due to Deccan volcanism.

Keywords: warming; benthic foraminifera; K/Pg extinction; plankton evolution; Paleocene; Paleogene.

1. Introduction

A series of perturbations of the global carbon cycle associated with global warming (hyperthermal events) punctuated the long-term warming trend of the early Paleogene (e.g., Thomas and Zachos, 2000; Cramer et al., 2003; Leon-Rodriguez and Dickens, 2010; Littler et al., 2014; Westerhold et al., 2018, 2020). The Paleocene-Eocene Thermal Maximum (PETM) was the largest of these events, while smaller hyperthermals occurred both before and after the PETM (e.g., Cramer et al., 2003; Dinarès-Turrell et al., 2014; Galeotti et al., 2015; Westerhold et al., 2018, 2020). Hyperthermals generally are modulated at astronomical frequencies, specifically eccentricity (e.g., Lourens et al., 2005; Westerhold et al., 2017, 2020; Barnet et al., 2019; Zeebe and Lourens, 2019). Paleocene hyperthermals

include the Lower C29n event (Coccioni et al., 2010), the Latest Danian Event (LDE, also called Top C27n event, Westerhold et al., 2008, 2011; Bornemann et al., 2009; Alegret et al., 2016) and the Early Late Paleocene Event (ELPE, also called Mid Paleocene Biotic Event, MPBE; Petrizzo, 2005; Bralower et al., 2006; Bernaola et al., 2007). The earliest Paleocene perturbation of the global carbon cycle is known as the Dan-C2 event (duration ~100 kyr), identified by Quillévéré et al. (2008) at ~65.2 Ma (Gradstein et al., 2004). In an updated calibration of the Upper Cretaceous–lower Eocene time scale (Barnet et al., 2019), Dan-C2 occurred ~160 kyr after the K/Pg boundary (66.0225 Ma; Dinarès-Turell et al., 2014), i.e., at ~65.86 Ma, the first 405-kyr Paleocene eccentricity maximum (Pc₄₀₅1) (Westerhold et al., 2011, 2020; Barnet et al., 2019).

Dan-C2 resembles hyperthermal events: negative excursions in $\delta^{13}\text{C}$ and $\delta^{18}\text{O}$ values in bulk sediment and in planktic foraminifera, and lower CaCO_3 concentrations in marine carbonate. The Dan-C2 event as observed at a few sites in the Atlantic Ocean is characterised by double, fairly symmetrical negative excursions in carbon and oxygen isotopes ($\delta^{13}\text{C}$ and $\delta^{18}\text{O}$) in bulk sediment, an increase in sediment clay content and a decrease in carbonate content (Kroon et al., 2007; Quillévéré et al., 2008; Barnet et al., 2017, 2019). The Dan-C2 was shorter than the PETM (Quillévéré et al., 2008), similar to post-PETM Eocene hyperthermals (e.g., Eocene Thermal Maximum 2, ETM2, Stap et al., 2009, 2010; Jennions et al., 2015; and Eocene Thermal Maximum 3, ETM3, Thomas et al., 2018). However, the event might have been restricted to the Atlantic and surrounding areas, including the Tethys Ocean (e.g., Westerhold et al., 2011). A Dan-C2 negative Carbon Isotope Excursion (CIE) was identified at ODP Hole 1049C (NW Atlantic) in bulk sediment (~1.3‰), planktic (~0.7‰) and benthic foraminifera (~1‰), and in bulk sediment in Deep Sea Drilling Project (DSDP) Holes 527 and 528 (SE Atlantic; ~1.5‰ and ~0.8‰ respectively) (Quillévéré et al., 2008). In the western Tethys (Gubbio section, Coccioni et al., 2010), Dan-C2 is observed in bulk $\delta^{13}\text{C}$ (~0.8‰) and $\delta^{18}\text{O}$ records, with a decline in CaCO_3 and in $\delta^{13}\text{C}$ data from a Ukrainian terrestrial setting (CIE of ~-3‰; Gilmour et al., 2013). The event was not identified at Site

1209 in the Pacific Ocean (Westerhold et al., 2011; Hull et al., 2020), nor Newfoundland Ridge Site U1403 (Hull et al., 2020). In contrast to other events, there was no deep-water warming recorded at any of these locations. At ODP Hole 1049C, there was ~4°C surface ocean warming as reconstructed from $\delta^{18}\text{O}$ values of bulk and planktic foraminifera, but no warming in the benthic record.

The event occurs at a 405-kyr eccentricity maximum, like later hyperthermal events (e.g., Lourens et al., 2005; Zeebe and Lourens, 2019; Westerhold et al., 2020). CIEs are generally related to the release of a large amount of ^{12}C -enriched carbon compounds into the ocean-atmosphere system, possibly through volcanic outgassing from Deccan Trap volcanism, but a volcanic origin would not explain the orbital pacing, and volcanic CO_2 does not have a sufficiently light isotopic signature (Barnet et al., 2017, 2019; Hull et al., 2020).

The PETM and other hyperthermals are characterised by increased clay and Fe concentrations in deep-sea sediments due to dissolution as a result of ocean acidification by the release of carbon compounds (Kroon et al., 2007; Speed and Kroon, 2000; Westerhold et al., 2008). However, low CaCO_3 levels in Dan-C2 may have been influenced by the fact that pelagic calcifiers (calcareous nannoplankton and planktic foraminifera) were not yet fully recovered from the K/Pg extinction (e.g., D'Hondt, 2005; Bernaola and Monechi, 2007; Birch et al., 2012, 2016; Alvarez et al., 2019). Its low carbonate concentration could have been due to low carbonate mass accumulation rates (Kroon et al., 2007) rather than to CaCO_3 dissolution (Barnet et al., 2019; Hull et al., 2020). The fine-grained carbonate in sediments directly above the K/Pg may have been produced not by calcareous nannoplankton, but by microbial 'whittings' (Bralower et al., 2020) and/or have an unknown, in part diagenetic origin (Minoletti et al., 2005).

Biotic turnover across the largest hyperthermal event, the PETM, has been extensively described, especially of deep-sea benthic foraminifera which underwent their largest extinction of the Late Cretaceous-Cenozoic (Tjalsma and Lohmann, 1983; Miller et al., 1987; Katz and Miller, 1991; Thomas, 1989, 1990a, b, 1998, 2007; Alegret et al., 2009a,

b, 2018; Hayek et al., 2019). Other marine and terrestrial groups show diversification, evolution of short-lived taxa, and/or migration to higher latitudes (e.g., McInerney and Wing, 2011; Speijer et al., 2012).

Benthic foraminiferal turnover across the smaller Paleocene - Eocene hyperthermals has been documented at fewer locations than the PETM. Assemblage changes are similar to those recorded across the PETM (low diversity and high dominance post-event), but there were no significant extinctions (D'haenens et al., 2012; Jennions et al., 2015; Alegret et al., 2016; Arreguín-Rodríguez et al., 2016; Arreguín-Rodríguez and Alegret, 2016; Thomas et al., 2018).

The response of benthic foraminifera to the Dan-C2 event has not been studied at sufficient time resolution and information is predominantly drawn from low-resolution data from studies on the K/Pg event (e.g., Alegret and Thomas, 2004, 2013), including at Site 1262 (Alegret and Thomas, 2007; Alegret et al., 2012). A low-resolution study of benthic foraminifera of the western Tethys Contessa Highway section reported increased abundance of opportunistic taxa, suggesting enhanced food flux to the seafloor and decreased oxygenation across Dan-C2 (Coccioni et al., 2010). We evaluate the benthic foraminiferal turnover at SE Atlantic ODP Site 1262 to investigate the paleoenvironmental and faunal response to the Dan-C2 event, over a time interval extending from 10.59 to 563.23 kyr after the K/Pg boundary.

2. Location and setting

Paleocene sediments at Ocean Drilling Program (ODP) Site 1262 (27°11.15'S, 1°34'2E; 3600 m paleodepth) in the Angola Basin, near the base of the north-western flank of Walvis Ridge (Figure 1) consist of brown calcareous clays with abundant nannofossils and planktic foraminifera (Zachos et al., 2004). The Dan-C2 event was recognised by a prominent double-spiked negative CIE in bulk sediment $\delta^{13}\text{C}$ values (Kroon et al., 2007;

Barnet et al., 2019), superimposed on a gradually decreasing trend in $\delta^{13}\text{C}$ between the K/Pg boundary and Dan-C2, with minimum values during the latter ($\sim 0.58\text{‰}$; Figure 2).

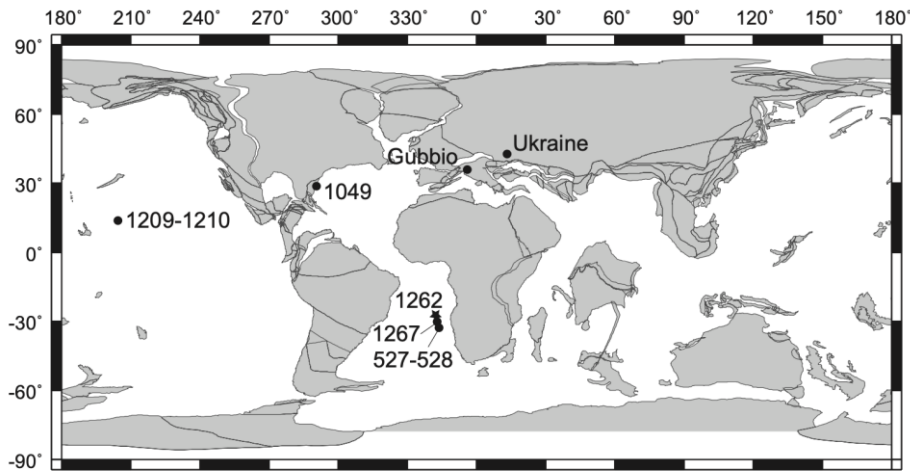


Figure 1. Paleogeographic reconstruction (65.2 Ma) showing the location of ODP Site 1262 and other sites mentioned in the text. Modified from Hay et al. (1999).

Both Site 1262 and the shallower Walvis Ridge Site 1267 show the double-spiked negative excursion in $\delta^{13}\text{C}_{\text{bulk}}$ values across Dan-C2 (Kroon et al., 2007; Hull et al., 2020; Figure 2), also seen at nearby DSDP Sites 527 and 528 (Quillévéré et al., 2008), and a gradual increase after the event, but no return to pre-excursion values in the studied interval. In contrast, $\delta^{13}\text{C}_{\text{benthic}}$ values decrease above the K/Pg, then are stable across Dan-C2, followed by a slightly decreasing trend up to the upper part of the studied section (213.7 meters composite depth, mcd) (Barnet et al., 2017, 2019; Figure 2). The $\Delta\delta^{13}\text{C}_{\text{(planktic-benthic)}}$ is reversed from normal (i.e., benthic values are heavier) from the K/Pg until ~ 100 kyr after Dan-C2.

The $\delta^{18}\text{O}_{\text{bulk}}$ values do not show a negative excursion during Dan-C2, and $\delta^{18}\text{O}_{\text{benthic}}$ values remain relatively stable, with a marked drop above it (215 mcd), reflecting similar values as in bulk sediment (Barnet et al., 2017, 2019; Figure 2). The CaCO_3 wt % shows the same pattern as bulk sediment $\delta^{13}\text{C}$ values, i.e., a decreasing trend below the event, minimum values during Dan-C2 ($\sim 5\%$) and a slight overall increase towards the upper part

of the studied interval (Alegret et al., 2012). The XRF-derived Fe intensity values mirror the %CaCO₃ trends, increasing from the lower part of the section up to Dan-C2, then slightly decreasing above the event, with two intervals of higher values coinciding with the two intervals with low CaCO₃ % (Figure 2).

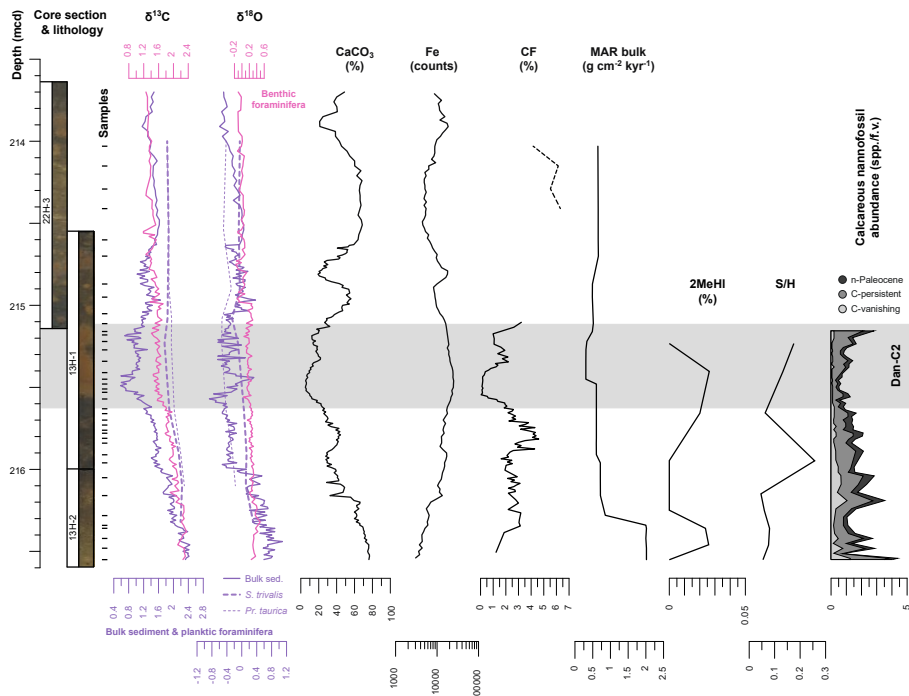


Figure 2. Stable isotope values ($\delta^{13}\text{C}$ and $\delta^{18}\text{O}$) of benthic foraminifera (*N. truempyi*; Barnet et al., 2017, 2019), bulk sediment (Kroon et al., 2007) and planktic foraminifera (Birch et al., 2016) at ODP Site 1262, compared with CaCO₃ content (Alegret et al., 2012), XRF-Fe counts (Westerhold et al., 2008), coarse fraction > 63 μm (CF; Barnet et al., 2019), and mass accumulation rates (MAR bulk). Biomarker data (2MeHI% and S/H; Bralower et al., 2020) and calcareous nannofossil abundance (Bernaola and Monechi, 2007) are shown to illustrate primary producers. The 2-methyl hopane index (2MeHI%) is indicative of cyanobacteria, and Sterane/Hopane (S/H) indicates the relative contribution of bacteria (H) and algae (S). Calcareous nannofossils: Cretaceous vanishing species (C-vanishing), Cretaceous-persistent species (C-persistent), and new Paleocene species (n-Paleocene). spp./f.v. = specimens per field of view. Grey area indicates the Dan-C2 event.

3. Methods

177

178 Samples were oven-dried at 50°C for 2–3 days, then weighed to obtain a bulk dry
179 sample weight, and soaked and disaggregated in a cold buffered sodium
180 hexametaphosphate ((NaPO₃)₆) solution for 12–24 hours. Then samples were sieved
181 through a 63 µm sieve to retain the coarse fraction and remove the fine clays and calcareous
182 nannofossils. The sieved samples were put onto a shaker table in a buffered (NaPO₃)₆
183 solution for 2 hours, to remove any further fines, then sieved a final time through a 63 µm
184 sieve. After a final rinse with ethanol to displace the water, samples were oven-dried at
185 50°C. The >63 µm sediment fraction was used for quantitative faunal analysis.

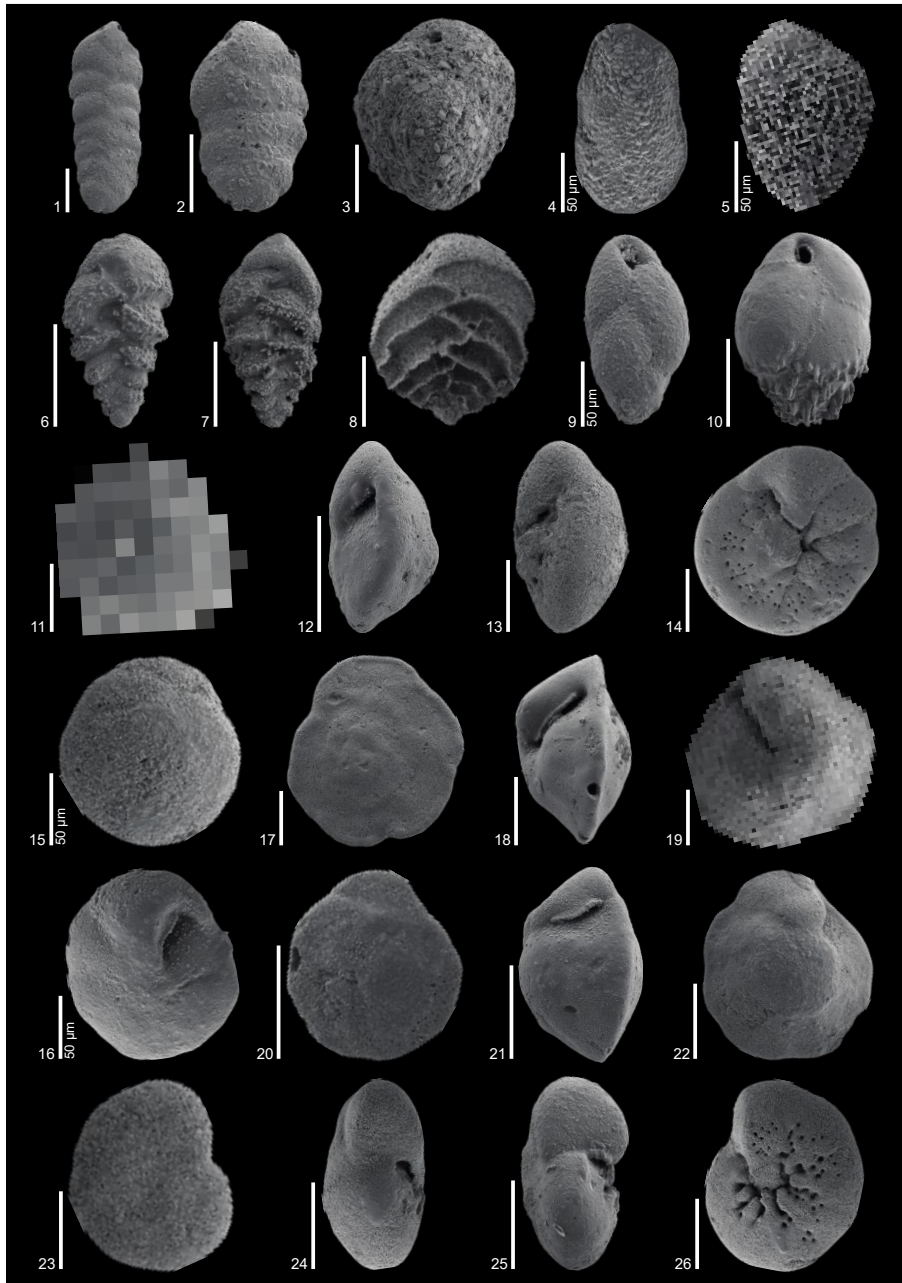
186 Benthic foraminifera were analysed in 39 samples from Cores 1262C-13H and
187 1262B-22H (216.55 – 214.03 mcd), 14 of which were studied by Alegret and Thomas
188 (2007), which encompass 552.64 kyr of the early Paleocene. We adjusted taxonomic
189 assignments following Arreguín-Rodríguez et al. (2018). The sampling resolution varies
190 from ~5–12 cm close to the event to up to ~20 cm towards the upper part of the studied
191 interval.

192 Approximately 300 specimens of benthic foraminifera were picked from each
193 sample (Table S1, Figures 3 and 4). For identification at the species and genus level we
194 followed Tjalsma and Lohmann (1983), Van Morkhoven et al. (1986), Loeblich and Tappan
195 (1988), and Alegret and Thomas (2001); for species that survive into the Eocene we
196 followed Arreguín-Rodríguez et al. (2018) and Hayward et al. (2012) for uniserial species
197 with complex apertures. A taxonomic reference list of common species (>2% of relative
198 abundance), including taxa cited in the text, is given in Table S2. Relative abundance of taxa,
199 diversity (Fisher-α index) and heterogeneity (Shannon-Weaver index) indices, as well as
200 the agglutinated-calcareous and infaunal-epifaunal ratios were calculated. The infaunal-
201 epifaunal ratio is based on the relation between morphology and microhabitat, and can be
202 used, with careful evaluation, as an approximate proxy for oxygenation and trophic
203 conditions at the seafloor (Jorissen et al., 1995, 2007). Additionally, we calculated the

percentage of buliminids *sensu lato* (s.l.) (Alegret and Thomas, 2013), excluding the superfamily Stilostomellacea. This group tolerates reduced oxygen conditions (Sen Gupta and Machain-Castillo, 1993) and/or thrives under abundant food supply (Thomas, 1998; Fontanier et al., 2002; Gooday, 2003; Jorissen et al., 1995, 2007).

The number of foraminifera per gram of dry sediment was calculated considering the sample-split weight used to pick benthic foraminifera. Bulk sediment accumulation rates (MAR_{bulk}) and benthic foraminiferal accumulation rates (BFAR) were calculated based on the average dry density for the studied interval (Zachos et al., 2004), and the age model in Barnett et al. (2019), which is orbitally tuned based on benthic $\delta^{13}C$ record and grounded with detailed magnetostratigraphic and biostratigraphic data. We used the number of specimens in the $>63 \mu m$ size fraction corrected to the weight of bulk sediment to estimate BFAR, which is a proxy to estimate the total organic matter flux to the seafloor (Herguera and Berger, 1991; Jorissen et al., 2007). The coarse fraction was determined as the weight ratio of $>63 \mu m$ size fraction to the bulk dry sediment weight.

R-mode hierarchical cluster analyses were performed to identify groups of species with similar distribution patterns. We used the unweighted pair-group average algorithm (UPGMA) and the Pearson correlation, as similarity coefficient. We performed detrended correspondence analyses (DCA) on R- and Q-modes to identify potential ecological variables that may have controlled the distribution of benthic foraminifera. A dataset of species with a relative abundance $>2\%$ in at least one sample (32 species) was constructed to perform cluster and DCA analyses. Some groups of taxa such as *Abyssammina* spp., *Anomalinoides* spp., *Chrysalogonium* spp., *Globulina* spp., *Gyroidinoides* spp., nodosariids, *Nuttallides* spp., *Nuttallinella* spp., *Osangularia* spp., *Paralabamina* spp., pleurostomellids and *Pyrulinoides* spp. were excluded from this dataset in order to compare exclusively single species.



229

230 Figure 3. SEM images of selected benthic foraminifera at ODP Site 1262. All scale bars represent 100
 231 μm, unless otherwise is indicated. 1 *Spiroplectammina spectabilis*, 215.27 mcd; 2 *Spiroplectammina*
 232 *spectabilis*, 215.27 mcd; 3 *Clavulinoides* sp., 215.53 mcd; 4 *Seabrookia cretacea*, 214.95 mcd; 5
 233 *Bolivina huneri*, 216.34 mcd; 6 *Tappanina eouvigeriniformis*, 216.34 mcd; 7 *Tappanina*
 234 *eouvigeriniformis*, 215.66 mcd; 8 *Aragonia ouezzanensis*, 214.03 mcd; 9 *Bulimina kugleri*, 214.95 mcd;
 235 10 *Bulimina midwayensis*, 215.41 mcd; 11 *Paralabamina hillebrandti*, 214.15 mcd; 12 *Paralabamina*
 236 *hillebrandti*, 214.15 mcd; 13 *Paralabamina hillebrandti*, 215.34 mcd; 14 *Paralabamina hillebrandti*,
 237 214.15 mcd; 15 *Nuttallinella rippleyensis*, 215.84 mcd; 16 *Nuttallinella rippleyensis*, 215.84 mcd; 17
 238 *Nuttallinella florealis*, 214.29 mcd; 18 *Nuttallinella florealis*, 214.29 mcd; 19 *Nuttallinella florealis*,

239 214.29 mcd; 20 *Nuttallides truempyi*, 215.81 mcd; 21 *Nuttallides truempyi*, 215.81 mcd; 22 *Nuttallides*
240 *truempyi*, 215.81 mcd; 23 *Stensioeina beccariiformis*, 216.34 mcd; 24 *Stensioeina beccariiformis*,
241 216.34 mcd; 25 *Stensioeina beccariiformis*, 215.16 mcd; 26 *Stensioeina beccariiformis*, 216.34 mcd.

242
243 Statistical analyses based on the comparison of samples from distinct time intervals
244 were performed in order to determine whether benthic foraminifera responded
245 significantly to the Dan-C2 event. We applied the Fligner-Killeen test (T), a nonparametric
246 test used to recognise equal coefficients of variation in two sample groups (Fligner and
247 Killeen, 1976), assuming that this measure of dispersion may reflect the stability of the
248 system (i.e., major variability points to unstable/perturbed systems and *vice versa*). The
249 intervals of time employed for these analyses were selected considering three alternatives:
250 the occurrence of the event (option A), a main change in diversity (option B), and a marked
251 change in faunal clusters (option C). In option A, the pre-event interval includes samples
252 from 216.55 to 215.66 mcd, and samples from 215.63 to 215.11 mcd correspond to Dan-C2.
253 For option B, the studied interval was divided in two parts: a lower (216.55 to 214.95 mcd)
254 and an upper part (214.87 to 214.03 mcd). In option C, the lower part includes samples from
255 216.55 to 215.81 mcd, and the upper part encompasses samples from 215.78 to 214.03 mcd.
256 We compared diversity and heterogeneity indices, relative abundance of agglutinated and
257 infaunal taxa, and the abundance of the faunal clusters. We used PAST software for the
258 statistical analyses (Hammer et al., 2001).

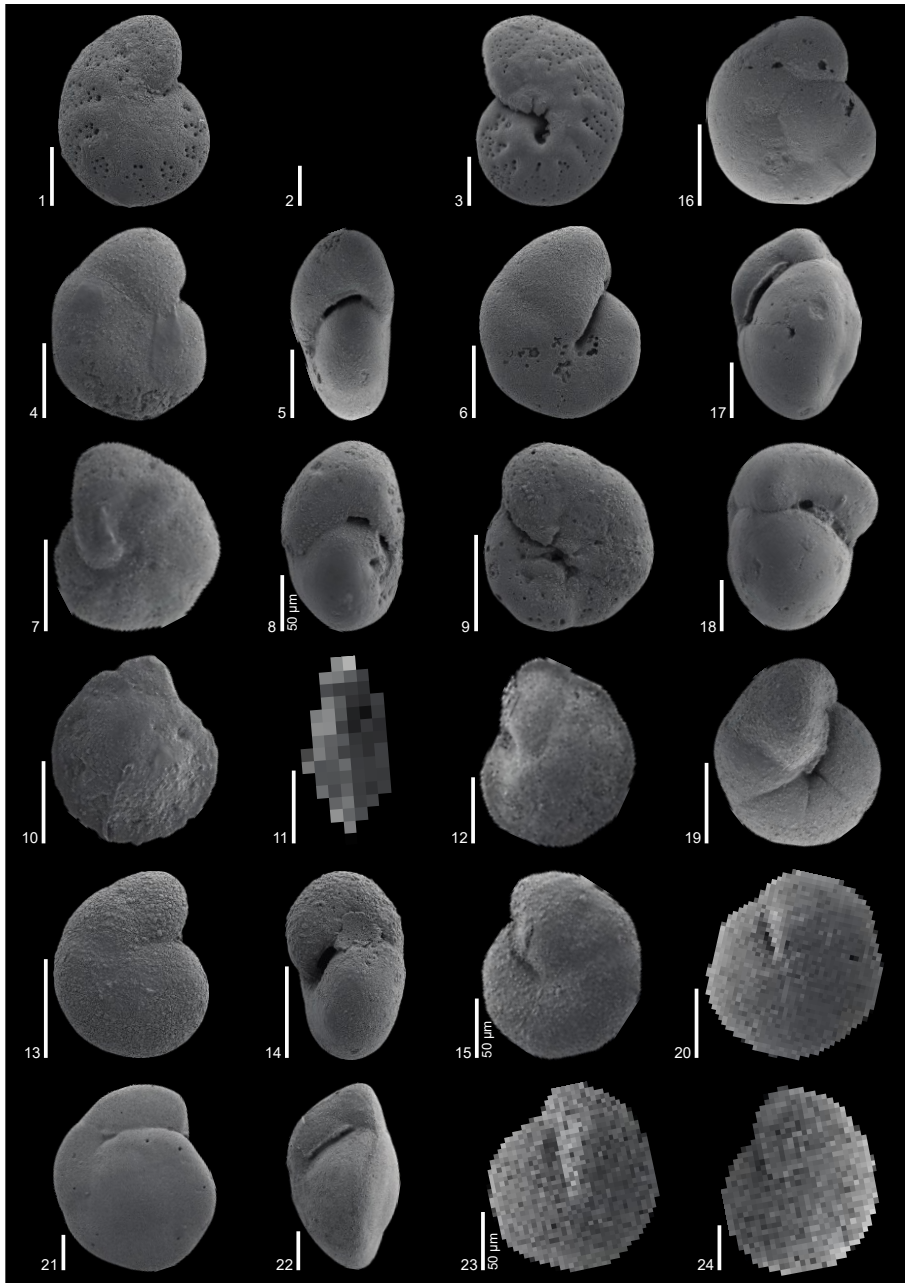


Figure 4. SEM images of selected benthic foraminifera at ODP Site 1262. All scale bars represent 100 μm, unless otherwise is indicated. 1 *Anomalinoides praeacutus*, 215.73 mcd; 2 *Anomalinoides praeacutus*, 215.57 mcd; 3 *Anomalinoides praeacutus*, 215.57 mcd; 4 *Abyssamina subplanispira*, 216.34 mcd; 5 *Abyssamina subplanispira*, 216.34 mcd; 6 *Abyssamina subplanispira*, 216.34 mcd; 7 *Cibicidoides hyphalus*, 214.15 mcd; 8 *Cibicidoides hyphalus*, 214.15 mcd; 9 *Cibicidoides hyphalus*, 214.15 mcd; 10 *Osangularia velascoensis*, 214.7 mcd; 11 *Osangularia velascoensis*, 215.27 mcd; 12 *Osangularia velascoensis*, 215.27 mcd; 13 *Gyroidinoides depressus*, 214.29 mcd; 14 *Gyroidinoides depressus*, 214.29 mcd; 15 *Gyroidinoides depressus*, 214.29 mcd; 16 *Gyroidinoides globosus*, 215.96 mcd; 17 *Gyroidinoides globosus*, 215.96 mcd; 18 *Gyroidinoides globosus*, 215.96 mcd; 19 *Gyroidinoides*

globosus, 215.66 mcd; 20 *Gyroidinoides globosus*, 215.96 mcd; 21 *Gyroidinoides beisseli*, 215.41 mcd; 22 *Gyroidinoides beisseli*, 215.41 mcd; 23 *Gyroidinoides beisseli*, 215.96 mcd; 24 *Gyroidinoides beisseli*, 215.41 mcd.

4. Results

4.1 Benthic foraminiferal assemblages and mass accumulation rates

The preservation of benthic foraminifera is generally good throughout the studied section (Figures 3, 4). Calcareous (average ~89%) and epifaunal (average ~56%) taxa dominate the assemblages (Table S1). The most abundant epifaunal taxa include the trochospiral *Stensioeina beccariiiformis* (average 10.8%), *Paralabamina hillebrandti* (average 6.3%) and *Nuttallinella rippleyensis* (average 5.7%). *Spiroplectammina spectabilis* (average 6.2%) is the most abundant infaunal species, which together with *Clavulinoides* spp. makes up the most abundant agglutinated taxa.

Diversity and heterogeneity are high at Site 1262, as expected for deep-sea faunas of the Late Cretaceous–Paleocene Velasco-type assemblage, but vary across the studied section. For a description of benthic foraminiferal assemblages, proxies and mass accumulation rates, the section was divided into three intervals, based on the recognition of Dan-C2 through the $\delta^{13}\text{C}$ record (Table 1). The pre-event interval includes samples from 216.55 to 215.66 mcd, the Dan-C2 interval samples from 215.63 to 215.11 mcd, and the post-event interval samples from 215.05 to 214.03 mcd.

The pre-event interval is characterised by strong fluctuations superimposed on a slight overall decrease in diversity and heterogeneity indices (Figure 5). BFAR values remain stable throughout this interval, increasing in its uppermost part, and reaching maximum values immediately below Dan-C2. The gradual increase in % agglutinated taxa correlates with a gradual decrease in %CaCO₃. The absolute abundance of benthic

foraminifera (Nr/gr) remains low, whereas taxa such as uniserial lagenids and polymorphinids decrease in abundance across this interval. Bolivinids s.s. peak in abundance in the lower part of the pre-event interval. Among the epifaunal taxa, *N. rippleensis* and *N. truempyi* decrease in abundance below Dan-C2, whereas *S. beccariiformis* increases. *Paralabamina hillebrandti* remains relatively stable, with a peak in abundance close to the base of Dan-C2. Bulk mass accumulation rates decrease markedly (from ~2 to 0.7 g cm⁻² kyr⁻¹) at 216.36–216.16 mcd, followed by a slight gradual decrease towards the upper part of the pre-event interval (Figure 2).

Table 1. Mean values of benthic foraminiferal indices, proxies and mass accumulation rates at pre-event, Dan-C2 and post-event intervals.

	Pre-event	Dan-C2	Post-event
BFAR	2151.0	1052.5	564.8
Diversity (Fisher- α)	19.4	17.7	21.1
Heterogeneity (H(S))	3.4	3.3	3.4
Foraminiferal density (Nr/gr)	76276.9	481652.1	11680.0
Agglutinated taxa (%)	8.8	14.2	11.5
Infaunal taxa (%)	47.1	39.8	46.3
Buliminids s.l. (%)	13.0	11.5	14.4
Buliminids s.s. (%)	4.5	5.3	7.0
Bolivinids s.s. (%)	5.2	3.9	4.3
Uniserial lagenids (%)	4.5	1.4	3.7
Stilostomellids (%)	0.8	0.3	1.3
Polymorphinids (%)	2.2	1.1	3.0
Unilocular taxa (%)	1.2	0.9	1.6
MAR _{bulk}	1.1	0.5	0.6

The Dan-C2 interval includes the lowest diversity values (Fisher- α ~13 at 215.45 mcd) and the highest absolute abundance of benthic foraminifera (215.51 mcd; Figure 5) due to the low coarse fraction, occurring during the lowest of the two negative $\delta^{13}\text{C}$ excursions. Diversity quickly recovers up-section, and a small peak in BFAR occurs in Dan-C2 (215.34 mcd). The increase in relative abundance of agglutinated species (up to ~22% of the assemblages) in the middle part of Dan-C2 is not coeval with the decrease in %CaCO₃,

and a linear regression analysis indicates that only 33% of the variability of agglutinated taxa is explained by variability of %CaCO₃ (Figure S1). Infaunal morphogroups, including uniserial lagenids, stilostomellids, polymorphinids and unilocular taxa, show their minimum in relative abundance across the event, whereas the epifaunal *S. beccariiformis* has its highest abundance in Dan-C2. Other taxa, such as *P. hillebrandti*, peak in abundance at the lowermost part of the event, and *N. rippleyensis* slightly increases towards the top of the event. Bulk mass accumulation rates, % calcium carbonate and coarse fraction reach their lowest values across Dan-C2 (Figure 2).

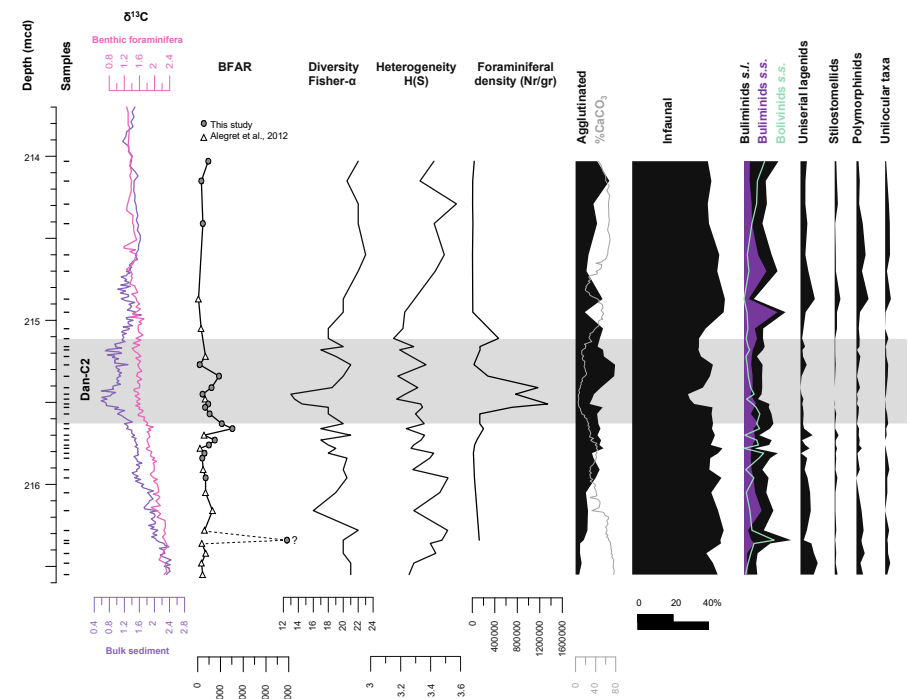


Figure 5. Benthic foraminiferal indices and proxies, including benthic foraminiferal accumulation rates (BFAR, including data from Alegret et al., 2012), diversity (Fisher- α), heterogeneity (Shannon-Weaver), foraminiferal density (N° specimens/gr dry sed.), relative abundance of agglutinated taxa, infaunal morphogroups, buliminids *sensu lato* (s.l.), buliminids *sensu stricto* (s.s.), boliviniids s.s., and other infaunal taxa (uniserial lagenids, stilostomellids, polymorphinids and unilocular taxa), compared to CaCO₃ content (Alegret et al., 2012), $\delta^{13}\text{C}$ values measured in *N. truempyi* (Barnet et al., 2017, 2019) and $\delta^{13}\text{C}$ in bulk sediment (Kroon et al., 2007).

Diversity and heterogeneity gradually increase above Dan-C2, towards the upper part of the studied interval (Figure 5). The percentages of some infaunal taxa (buliminids s.s., uniserial lagenids, polymorphinids, stilostomellids and unilocular taxa) slightly increase above Dan-C2, whereas agglutinated taxa slightly decrease. Relative abundance of some epifaunal taxa gradually decreases above Dan-C2 (*S. beccariiiformis*), and that of others increases towards the upper part of the studied section (e.g., *N. truempyi*, *N. rippleyensis*). BFAR and absolute abundance values decrease and are similar to pre-event values, and bulk mass accumulation rates remain low (Figure 2).

4.2 Faunal clusters and DCAs

The dendrogram of the R-mode cluster analysis shows two main clusters of benthic foraminiferal species (Figure 6). Cluster A is divided into subclusters A1 and A2, and it is composed of epifaunal and infaunal taxa. Subcluster A1 is dominated by *Nuttallinella rippleyensis*, *Nuttallides truempyi* and *Paralabamina lunata*, and is most abundant in the pre-event interval (up to sample 215.81 mcd); its abundance decreases towards Dan-C2 and increases slightly above the event (Figure 6). *Bulimina kugleri*, *Seabrookia cretacea* and *Oridorsalis umbonatus* are the most abundant species of subcluster A2, which contains exclusively infaunal taxa that increase in abundance above Dan-C2 (214.60-215.05 mcd), remaining fairly stable in the interval below and across Dan-C2.

Cluster B, subdivided into subcluster B1 and subcluster B2, consists of mixed infaunal and epifaunal taxa, including species that dominate the assemblages (and/or increase in abundance) in Dan-C2. Subcluster B1 is mostly composed of epifaunal taxa, except for the infaunal agglutinated species *Spiroplectammina spectabilis* and *Clavulinoides* sp. This is the most abundant subcluster, and it gradually increases from the interval below the event towards Dan-C2 (Figure 6). *Stensioeina beccariiiformis*, *S. spectabilis* and *Paralabamina hillebrandti* are the most abundant species. Less abundant subcluster B2

shows minor abundance peaks below and within Dan-C2 (215.41–215.81 mcd; Figure 6). The most abundant species of this subcluster are infaunal *Tappanina eouvigeriniformis* and epifaunal-shallow infaunal *Gyroidinoides beisseli*.

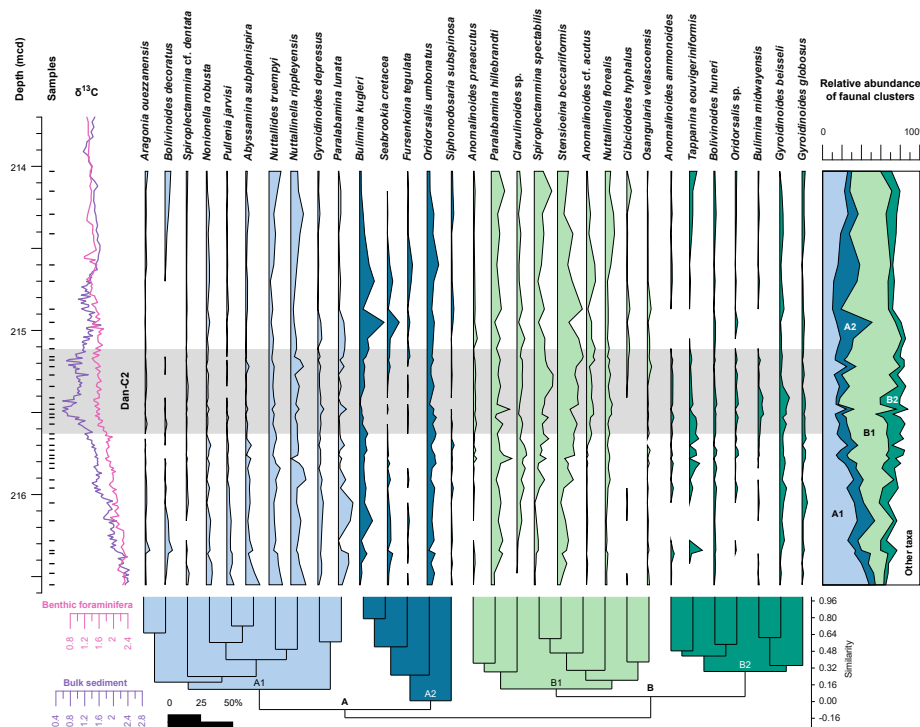


Figure 6. R-mode dendrogram and relative abundances of selected benthic foraminiferal taxa and faunal clusters across the lower Paleocene at ODP Site 1262, plotted against $\delta^{13}\text{C}$ values measured in *N. truempyi* (Barnet et al., 2017, 2019) and in bulk sediment (Kroon et al., 2007).

Cluster B species are located at lower values along axis 1 in the R-mode DCA plot (Figure 7A), whereas cluster A score middle-high values on this axis. Most species are placed at middle values along axis 2, but subclusters A1 and B2 include taxa at the lowermost values of this axis (*Bolivinoidea decoratus*, *T. eouvigeriniformis*). Species from subcluster A2, particularly infaunal *Fursenkoina tegulata* and *S. cretacea*, score the highest values along the vertical axis (axis 2).

Samples representing Dan-C2 are located towards the left of the Q-mode DCA plot (Figure 7B), i.e., at lowest values along axis 1, except for samples at 215.22 and 215.48 mcd,

which score middle values. Most samples above the event are at low-medium values along the horizontal axis (axis 1). Samples below the event show a wide range of values, with those corresponding to >216 mcd reaching higher values along axis 1.

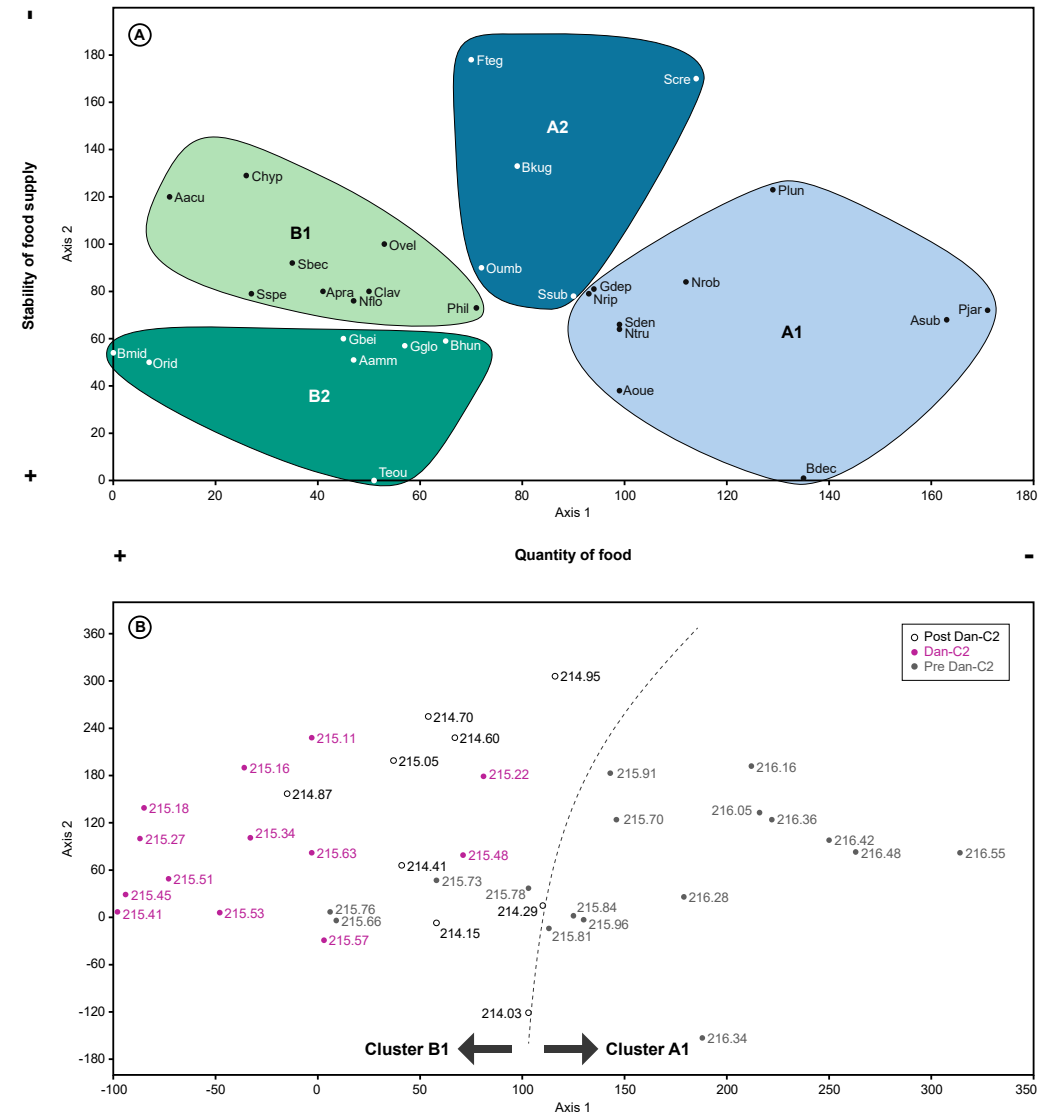


Figure 7. Detrended correspondence analysis (DCA) results. A) R-mode (species) plot. The outlined groups represent faunal clusters (A1, A2, B1, B2) and the bars along the axes indicate the overall ecological preferences of the taxa. Full names are written in Table S2. B) Q-mode (samples) plot. The dashed line separates samples depending on their faunal content: samples to the right are dominated by species from cluster A1, and to the left by species from cluster B1.

4.3 Testing the coefficient of variation

We statistically compared several variables between intervals before and during Dan-C2 (Table 2). Neither diversity, heterogeneity nor faunal clusters (A1, A2 and B2) show significant differences in coefficient of variation among those intervals, but agglutinated species, infaunal taxa and cluster B1 show a statistically distinctive coefficient of variation (p -values <0.05). Coefficients of variation of agglutinated taxa and cluster B1 decrease in Dan-C2, indicating less variability thus more steady values during the event. In contrast, the coefficient of variation of infaunal taxa increases in Dan-C2, reflecting more fluctuating values (Figure 8).

Table 2. Results of Fligner-Killeen tests based on the Dan-C2 event (option A).

	Option A	CV	T test	p -value
Diversity	Dan-C2	14.545	15.1590	0.06589
	Pre-event	8.698		
Heterogeneity	Dan-C2	2.361	8.8803	0.25810
	Pre-event	2.747		
Agglutinated	Dan-C2	30.068	4.9910	0.02377
	Pre-event	54.075		
Infaunal	Dan-C2	12.619	18.7410	0.00317
	Pre-event	6.275		
Cluster A1	Dan-C2	26.181	6.8086	0.08711
	Pre-event	33.377		
Cluster A2	Dan-C2	39.392	13.6600	0.16140
	Pre-event	29.631		
Cluster B1	Dan-C2	11.855	2.3049	0.00186
	Pre-event	39.918		
Cluster B2	Dan-C2	47.976	7.0882	0.10329
	Pre-event	64.504		

We thus do not observe a clear response of benthic foraminifera to Dan-C2. We applied this test to other depth (thus time) intervals where we noted changes in diversity and heterogeneity (option B), and changes in relative abundance of clusters (option C; Figure 8). In option B, no variables show statistically significant differences (Table 3); whereas option C shows significant differences in coefficients of variation of the diversity

index, agglutinated taxa, and clusters B1 and B2. Such differences are associated with higher coefficients of variation of these variables (except for the diversity index) in the lower interval, which imply more variability, and thus more unstable conditions across this interval (Table 4, Figure 8).

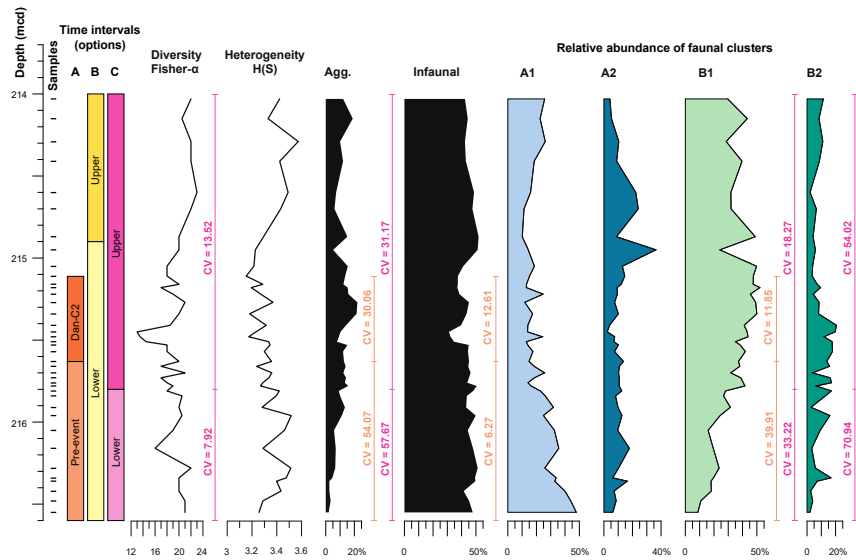


Figure 8. Time intervals and variables used in the Fligner-Killeen test. Intervals are based on the occurrence of Dan-C2 (option A, orange), main change in diversity (option B, yellow) and change in dominance of faunal clusters (option C, pink). Coefficients of variation (CV) are indicated next to the variable, when comparison of such variable between intervals is statistically different.

Table 3. Results of Fligner-Killeen tests based on main changes in diversity (option B).

	Option B	CV	T test	p-value
Diversity	Upper	4.756	1.6403	0.06797
	Lower	11.699		
Heterogeneity	Upper	2.734	4.8405	0.40012
	Lower	2.947		
Agglutinated	Upper	37.964	3.7844	0.25455
	Lower	47.196		
Infaunal	Upper	8.117	3.3981	0.20918
	Lower	12.276		
Cluster A1	Upper	35.116	4.9579	0.41772
	Lower	43.362		
Cluster A2	Upper	66.204	9.1359	0.08028

	Lower	53.241		
Cluster B1	Upper	21.353	2.4768	0.12212
	Lower	36.974		
Cluster B2	Upper	45.701	4.6204	0.36772
	Lower	58.758		

Table 4. Results of Fligner-Killeen tests based on marked changes in faunal clusters (option C).

	Option C	CV	T test	p-value
Diversity	Upper	13.523	4.6125	0.04418
	Lower	7.924		
Heterogeneity	Upper	3.004	9.4955	0.42820
	Lower	2.748		
Agglutinated	Upper	31.173	18.2050	0.00575
	Lower	57.674		
Infaunal	Upper	12.570	5.1348	0.06216
	Lower	6.692		
Cluster A1	Upper	27.943	7.4796	0.20961
	Lower	23.473		
Cluster A2	Upper	61.723	7.3679	0.19976
	Lower	35.930		
Cluster B1	Upper	18.271	17.5000	0.01049
	Lower	33.221		
Cluster B2	Upper	54.020	16.3610	0.02536
	Lower	70.946		

5. Discussion

5.1 Paleoecological inferences

We use the results of the multivariate analysis to infer changes in ecological conditions. Using the R-mode DCA plot and ecological preferences of taxa as derived from the literature, we interpret these axes as related to food availability (e.g., quantity, stability) to benthic foraminifera (Figure 7A). No evidence has been found to suggest other parameters (e.g., oxygenation, carbonate saturation or bottom current strength) as limiting

factors for benthic foraminiferal assemblages across the studied interval (see section 5.2 for further details).

Horizontal axis 1 may indicate the overall amount of food, with less food availability at higher values, where some oligotrophic species plot, such as *N. truempyi*, *N. rippleyensis*, *A. subplanispira* and *P. lunata* (subcluster A1; e.g., Alegret and Thomas, 2009; Deprez et al., 2015). Somewhat more eutrophic taxa (e.g., *S. beccariiiformis*, *A. acutus*, *A. praeacutus*, *Bulimina* spp.; e.g., Thomas, 1998; Jorissen et al., 2007; Alegret et al., 2021) are at lower values along the axis. We note that some taxa generally deemed oligotrophic (*C. hyphalus* and *N. florealis*; e.g., Widmark and Malmgren, 1992; Alegret and Thomas, 2005) occur at lower values on axis 1, and some species potentially linked to high food supply (*P. jarvisi*; e.g., Arreguín-Rodríguez and Alegret, 2016) at higher values, but these species are not abundant.

The distribution of species along the vertical axis (axis 2) may be related to the stability of the food supply, with high values representing a more pulsed or variable supply, and low values indicating stable conditions. *Seabrookia cretacea* and *B. kugleri* (subcluster A2) are at high values along axis 2 (Figure 7A), and may be opportunists responding to a pulsed food input (e.g., Alegret and Thomas, 2005; Sprong et al., 2013), possibly similar to *Seabrookia rugosa* (Thomas et al. 2018). *Paralabamina lunata* (high values along axis 2) is indicative of more oligotrophic conditions (e.g., Alegret and Thomas, 2005; Mello et al., 2017), and may have been able to feed on a specific type of food (Alegret and Thomas, 2013), e.g., more labile phytodetritus (Deprez et al., 2017). The position of *B. decoratus* at the lowermost values along axis 2 may support this interpretation, since buliminids are typically related to consistent trophic conditions (e.g., Jorissen et al., 1995, 2007; Gooday, 2003; Alegret and Thomas, 2009). *Bolivinooides crenulata* and *B. huneri*, which resemble *B. decoratus* in morphology (Arreguín-Rodríguez et al., 2018), might indicate a lower food flux than other buliminids, or a flux stabilised by a more refractory input (Fenero et al., 2012; Boscolo Galazzo et al., 2013, 2015; Arreguín-Rodríguez et al., 2018). *Tappanina*

eouvigeriniformis is indicative of higher organic flux to the seafloor (Alegret and Thomas, 2013), and plots at similarly low values along the vertical axis as *B. decoratus*, thus may indicate an overall higher food flux at similar stability.

In the Q-mode plot, samples from Dan-C2 and post-event interval plot at low values along axis 1 (Figure 7B), and are dominated by subcluster B1 (mainly *S. beccariiiformis* and *S. spectabilis*). Dan-C2 samples reach the lowest values on axis 1, but two samples (215.22 and 215.48 mcd) are located at about the middle of this axis. These samples have small peaks in abundance of subcluster A1 species (*N. rippleyensis* or *P. lunata*), which have a lower abundance in other Dan-C2 samples.

Most samples from below Dan-C2 (pre-event interval) plot at higher values along axis 1, with a high percentage of subcluster A1 species (*N. truempyi*, *N. rippleyensis*). Benthic foraminiferal assemblages changed markedly ~117 kyr after the K/Pg (215.81 mcd), with lower samples (216.55 – 215.81 mcd) having common subcluster A1 species (oligotrophic). Subcluster B1 species are more abundant from 215.78 to 214.03 mcd (higher trophic conditions). We thus suggest that there was more extreme variability in food (thus stress) in the lower part of the studied interval (~117 kyr after the K/Pg, prior to Dan-C2), followed by more stable conditions, even in Dan-C2, although stressful environments persisted until at least ~368 kyr after the K/Pg (sample 214.95 mcd; Figure 5; Alegret and Thomas, 2007; Bralower et al., 2020). Factors associated to these unstable conditions are discussed on section 5.2.

5.2 Paleoenvironmental interpretation

The dominance of well-preserved calcareous benthic foraminiferal taxa indicates deposition well above the carbonate compensation depth. The lack of carbonate dissolution is also supported by linear regression analysis showing that only 33% of the variability of agglutinated taxa depends on %CaCO₃ (Figure S1). The sediments deposited during the first

1–2 million years of the Paleocene are clay rich (60–80 wt % CaCO_3 ; Zachos et al., 2004), and have high XRF-derived Fe intensity at low sedimentation rates, indicating a lack of dilution by clays (Barnet et al., 2019). CaCO_3 wt. % declined precipitously at the K/Pg boundary with the mass extinction of pelagic calcifiers, then further declined gradually up-section to reach a minimum (~5%) at Dan-C2 (Figure 2). In Dan-C2 planktic foraminifera are rare, as shown by a low CaCO_3 wt % combined with minimum values of % coarse fraction (Thomas et al., 2007; Figure 2). The persistently low CaCO_3 wt. % over the studied interval at Site 1262 (Zachos et al., 2004) is probably due to a persistently low supply of carbonate produced by pelagic calcifiers after their extinction at the K/Pg mass extinction (e.g., D'Hondt, 2005; Alegret et al., 2012; Alvarez et al., 2019). The pattern of somewhat higher CaCO_3 wt. % just above the boundary followed by a decline is seen at several sites, and explained as due to microbial (not eukaryote) carbonate production directly after the asteroid impact (Sepulveda et al., 2019; Bralower et al., 2020). The organic matter produced by prokaryotes (e.g., similar to the extant *Synechococcus* and *Prochlorococcus*), however, may have been transported to the seafloor less efficiently than carbonate-ballasted organic matter (Bralower et al., 2020).

The benthic foraminiferal morphogroups point to meso-oligotrophic conditions, with a flux of organic matter to the seafloor sufficient to sustain both epifaunal and infaunal taxa (e.g., Jorissen et al., 1995). There is no organic enrichment or lamination in the sediments, and we see no high abundances of oxygen-tolerant taxa even in the samples with lowest diversity, so we conclude that oxygenation was not a limiting factor. Fluctuations in diversity and heterogeneity of the assemblages in the intervals before and during Dan-C2 (Figure 5) suggest environmental stress at the seafloor, possibly related to instability and heterogeneity of primary productivity after the K/Pg impact event (Hull and Norris, 2011; Alegret et al., 2012), as controlled by ecological processes and not by proximity to the impact site (Lowery et al., 2018; Bralower et al., 2020). Some argue for a fast recovery of primary productivity after the K/Pg, at least locally or regionally (e.g., Sepulveda et al., 2009;

Lowery et al., 2018; Henehan et al., 2019; Schaefer et al., 2020), though others indicate a more gradual and prolonged re-establishment of diverse ecosystems (e.g., Alvarez et al., 2019), and possibly increased roles for mixotrophic forms rather than photosynthesizers (Gibbs et al., 2020). It may well be that we see major regional heterogeneity in primary productivity after the K/Pg (e.g., Alegret et al., 2012; Esmeray-Senlet et al., 2015; Henehan et al., 2019), so that the tempo of recovery is not the same globally.

Re-establishment of diverse ecosystems of pelagic calcifiers may have been affected and/or delayed by ongoing CO₂ emissions from Deccan volcanism (e.g., Hull et al., 2020). At Walvis Ridge, evidence from calcareous nannofloras and planktic foraminifera as well as planktic $\delta^{13}\text{C}$ records shows that high variability in pelagic ecosystems, thus probably in export of organic matter to the sea floor, persisted for more than 1 million years after the K/Pg, extending beyond our studied interval (Bernaola and Monechi, 2007; Schueth et al., 2015; Birch et al., 2016; Figure 2).

Low BFAR values prevailed throughout the studied section (Figure 5), pointing to low export productivity. Small peaks in BFAR (samples 215.66 and 215.34 mcd) indicate a transient increase in export productivity, possibly due to lateral terrigenous input with refractory organic matter, although we did not observe an increase in MAR_{bulk}. A relatively low but variable input of organic matter to the seafloor is compatible with the common occurrence of oligotrophic species such as *N. truempyi*, *A. subplanispira* and *P. lunata* (subcluster A1), as well as with the scattered peaks in relative abundance of the more eutrophic buliminid group (Thomas et al., 2000; Alegret and Thomas, 2009; Deprez et al., 2015) in the interval below Dan-C2 (below 215.78 mcd, Figures 5, 6). Our data on fluctuations in the diversity and heterogeneity indices, and the abundance peaks of some taxa (e.g., buliminids *s.l.*) suggest that benthic foraminiferal assemblages remained disturbed until ~ 389 kyr after the KPg. Towards the upper part of the studied section (i.e., ~389 to ~563 kyr after the K/Pg, 214.87 to 214.03 mcd), the assemblages started to stabilise, diversity and heterogeneity indices gradually increased, and infaunal taxa other

than buliminids *s.l.* (such as uniserial lagenids, polymorphinids, stilostomellids and unilocular taxa) increased in relative abundance.

Towards the Dan-C2 event, *N. truempyi* decreased in abundance and *S. beccariiformis* (subcluster B1) increased. The species *S. beccariiformis* generally was more abundant at somewhat shallower depths than *N. truempyi* (e.g., Tjalsma and Lohmann, 1983; Widmark and Malmgren, 1992; Thomas, 1990a, b; Alegret et al., 2009a, b; Arreguín-Rodríguez et al., 2018), although *S. beccariiformis* extended its range into deeper waters at the K/Pg extinction (Alegret et al., 2012). This species has been found to thrive under oligotrophic, well-oxygenated conditions during the Late Cretaceous (e.g., Friedrich and Hemleben, 2007), but its negative correlation to the highly oligotrophic *N. truempyi* (e.g., Sites 1210 and 690; Alegret and Thomas, 2009, 2013) suggest that this species requires a higher food supply than *N. truempyi* (e.g., Widmark and Malmgren, 1992; Thomas et al., 2000). Thus, we interpret the increase in %*S. beccariiformis* and decrease in %*N. truempyi* towards Dan-C2 as the probable development of slightly more eutrophic conditions at the seafloor.

On the other hand, the increase in *S. beccariiformis*, a heavily calcified species which became extinct during the PETM whereas *N. truempyi* survived that ocean acidification event, has been linked to a higher carbonate saturation state after the K/Pg mass extinction of pelagic calcifiers (Alegret and Thomas, 2007), due to decreasing output of carbonate from the oceans while input did not decrease (e.g., Henahan et al., 2019; Bralower et al., 2020). Linear regression tests, however, indicate a significant but low correlation ($R^2 = \sim 40\%$ or less, Figure S1) between %CaCO₃ and diversity, heterogeneity, uniserial lagenids, polymorphinids and unilocular taxa, suggesting that perturbation of benthic foraminiferal assemblages was not exclusively associated with the recovery of calcareous plankton (thus declining deep ocean carbonate saturation state) and its potential influence on the efficiency of the biological pump, thus overall food supply.

The increased abundance of agglutinated taxa in Dan-C2 was largely due to the proliferation of infaunal *S. spectabilis*. This species agglutinates using carbonate (Kaminski and Gradstein, 2005), thus its proliferation was not caused by carbonate dissolution. In addition, we observed that CaCO_3 saturation increased, based on the dominance of calcareous benthic taxa across the low $\%\text{CaCO}_3$ interval, and on the common occurrence of the heavily calcified *S. beccariiformis*. *Spiroplectammina spectabilis* is commonly regarded as a 'disaster taxon', blooming in the presence of an increased food supply (Kaminski and Gradstein, 2005; Alegret et al., 2003), and we note the decreased abundance of oligotrophic *N. truempyi* towards the Dan-C2 event, which supports this interpretation.

Other infaunal taxa such as buliminids *s.l.* (mainly *B. kugleri*) and *S. cretacea* (cluster A2) increased in abundance after Dan-C2 (214.95 mcd, Figure 6). *Bulimina kugleri*, like other buliminids and infaunal taxa, has been related to a high food supply (e.g., Alegret and Thomas, 2009) even in the absence of clear indicators of low-oxygen conditions at the seafloor (Sen Gupta and Machain-Castillo, 1993). The species bloomed after the K/Pg boundary in the NE Atlantic (Alegret and Thomas, 2004) and after the extinction event at the PETM in the Southern Ocean (e.g., Thomas, 2003), suggesting opportunistic behaviour. The lack of a coeval increase in BFAR (Figure 5) points to a change in the nature of the food supply rather than to a net increase in the total amount of organic matter reaching the seafloor. We argue that the evolution of new species and varying productivity by different groups of primary producers during the early Paleogene may have caused variability in the type of food supply to the seafloor (Bralower et al., 2020; Figure 2), so that benthic opportunistic taxa (buliminids *s.l.*, *S. cretacea*) may have had an ecological advantage.

5.3 Dan-C2 event

Our results confirm that Dan-C2 differs materially from typical Paleogene hyperthermals (e.g., PETM, ETM2, ETM3; Littler et al., 2014; Barnet et al., 2019) in the minor

response of benthic foraminifera (even as compared to the smaller Eocene hyperthermals), probably related to the lack of bottom water warming (Figure 2). There is considerable evidence that bottom water warming caused a lower supply of food to the benthos due to increased mineralization of organic matter (e.g., Jennions et al., 2015; Thomas et al., 2018; Griffith et al., 2021).

There are no major differences in the structure or composition of the assemblages before and during Dan-C2, and the minor changes do not support the occurrence of a major ecological perturbation in the deep-sea. This lack of response is documented by the results of the Fligner-Killeen test (option A, Table 2), which indicates that samples from the Dan-C2 interval do not show significant evidence of perturbation. The relative abundance of agglutinated taxa and cluster B1 show statistically significant differences between assemblages before and during the event, with higher values of the coefficient of variation before the event indicating more instability of the assemblages. Similarly, a comparison of time intervals based on the main change in faunal clusters (option C), also shows that the diversity index and the relative abundance of agglutinated taxa, clusters B1 and B2 have significantly higher coefficients of variation in the lower interval (i.e., before Dan-C2; Figure 8). Only infaunal taxa show a higher coefficient of variation during the Dan-C2 event (Figure 8), possibly related to changing trophic conditions at the seafloor (i.e., an increase in input of food during Dan-C2). Our data indicate that benthic foraminifera underwent more environmental stress before the Dan-C2 event than during the event, in agreement with Alegret and Thomas (2007). Possibly, the food supply increased during Dan-C2 because of surface (though not deep-sea) warming, which caused intensification of the hydrological cycle as during the PETM (e.g., McNerney and Wing, 2011), thus more intense weathering on land, delivering more nutrients and resulting in increased primary productivity, while the lack of warming deeper in the water column meant that the food was delivered to the benthos, and not remineralized (Griffith et al., 2021).

Benthic foraminifera across Dan-C2 have been scarcely studied so far, with information available from the Italian Gubbio section only (Coccioni et al., 2010). This record, and our results, both show minor changes in benthic assemblages during the event, with agglutinated taxa slightly increasing in relative abundance. Coccioni et al. (2010) linked the faunal turnover to carbonate dissolution, because of higher values of the planktic fragmentation index, whereas we see no such evidence at Site 1262. These authors noted an increase in the absolute abundance of benthic foraminifera across Dan-C2, which they interpreted as a recovery of the food web and/or enhanced eutrophication, similar to what we observed, and possibly likewise the result on an increased hydrological cycle due to surface warming,

The occurrence of Dan-C2 during an eccentricity maximum strongly suggests that this event, though fundamentally different from later hyperthermal events in environmental and ecological expression (e.g., a lack of deep-sea warming, geographically different bulk $\delta^{13}\text{C}$ records), had similar causal mechanisms. All Paleogene hyperthermals, occurred at specific orbital configurations, i.e., at maxima in the 405 kyr eccentricity (e.g., Lourens et al., 2005; Zeebe and Lourens, 2019; Westerhold et al., 2020).

The precise causal mechanisms of the orbital triggering are not known and strongly debated: e.g., an orbitally-triggered process of release of isotopically light carbon from the lithosphere into the ocean-atmosphere system through dissociation of gas hydrates (e.g., Dickens, 2011) or decomposition of soil organic carbon in circum-Arctic and Antarctic terrestrial permafrost, as proposed by DeConto et al. (2012). The environmental (thus isotopic) expression of the Dan-C2 event may have differed from that of typical hyperthermals, because a release of carbon compounds occurred at a time when the global carbon cycle functioned very differently than later in the Paleogene (e.g., Barnet et al., 2019), due to its major disruption by the loss of functional pelagic calcifiers. This extinction changed the oceans from a so-called 'Cretan' state of low saturation dominated by biogenic pelagic CaCO_3 precipitation, back to a 'Neritan' state of indefinite saturation with only

shallow-water biogenic CaCO_3 precipitation (Zeebe and Westbroek, 2003; Ridgwell, 2005; Ridgwell and Zeebe, 2005). If the oceans were carbonate-oversaturated at the time of Dan-C2 because pelagic calcifiers had not fully recovered from the K/Pg extinction, even a large CO_2 release (from the Deccan Traps, e.g., Henehan et al., 2019; Hull et al., 2020, or another source releasing carbon at orbital periodicity) may not have had a major effect on deep-sea carbonate saturation.

Dan-C2 represents a carbon cycle perturbation at the same orbital configuration as Paleogene hyperthermals, but we think that it cannot be considered a true hyperthermal event because it was not global in extent, there was no deep-sea warming or carbonate dissolution, and a lack of response in deep-sea benthic foraminifera. Therefore, we suggest that Dan-C2 for now should be considered as an eccentricity-linked carbon cycle disturbance (ELCD). Possibly, negative excursions in planktic and bulk $\delta^{18}\text{O}$ do not indicate surface warming, because they can have been affected by differences in diagenesis during and outside the event, or by changes in surface ocean salinity, e.g., due to alterations in the evaporation/precipitation balance. We thus need to confirm whether there was surface ocean warming during Dan-C2, and if so, how much, using independent temperature proxies such as Mg/Ca in carbonate or organic biomarker-derived proxies. Alternatively, the nature of the Dan-C2 event was modified because of its occurrence in a world in which the oceanic carbon cycle was affected by a lack of abundant oceanic calcifiers.

6. Conclusions

Analysis of benthic foraminifera at Walvis Ridge ODP Site 1262 (SE Atlantic) reveals unstable environmental deep-sea floor conditions during the early Paleogene, probably related to changes in calcareous and non-calcifying primary producers as a long-term effect of the K/Pg mass extinction, potentially affected by CO_2 -release from continuing Deccan volcanism. Such volcanic activity could have affected sea-surface biota which had not yet

recovered from the K/Pg extinction. We suggest that these changes triggered variability in the quantity, stability and type of food arriving at the seafloor. Benthic foraminiferal assemblages indicate a gradual improvement in trophic conditions towards the upper part of the studied interval: environmental stress was most significant up to ~117 kyr after the K/Pg (215.81 mcd), when assemblages were dominated by species from cluster A1, followed by less perturbed conditions (dominance of cluster B1; up to ~368 kyr after the K/Pg; 214.95 mcd), and finally stabilization of the food supply at ~65.633 Ma (~389 kyr after the K/Pg; 214.87 mcd).

The Dan-C2 event, an eccentricity-linked carbon cycle disturbance, cannot be considered as a hyperthermal event because of the lack of bottom water warming, a lack of evidence of surface water warming on a global scale, a lack of evidence for widespread deep-sea dissolution, and a lack of significant changes in benthic foraminiferal assemblages. More evidence is needed, however, to define how widespread surface warming was. We agree with earlier suggestions that Dan-C2, though it occurred at a similar orbital configuration as later hyperthermals, may have had a very different expression (isotopically and environmentally) because of the fundamentally different carbonate saturation state of the oceans caused by long-term effects of the mass extinction of pelagic calcifiers at the K/Pg boundary.

Acknowledgements

G.J.A.R. and L.A. acknowledge funding from projects CGL2017-84693-R and PID2019-105537RB-I00 (Spanish Ministry of Science and Innovation and FEDER funds), and from Consolidated Group E05 (Government of Aragon/Fondo Europeo de Desarrollo Regional). E.T. recognises partial funding by NSF_OCE 1536611. G.J.A.R thanks the Consejo Nacional de Ciencia y Tecnología (Conacyt, México) for her predoctoral fellowship. J.S.K.B. and K.L. acknowledge funding from the Natural Environment Research Council (NERC)

Isotope Geosciences Facility at the British Geological Survey (IP-1581–1115) and D.N.S. support from the Royal Society via Wolfson Merit award. This research used samples provided by the Ocean Drilling Program (ODP), sponsored by the U.S. National Science Foundation (NSF) and participating countries under management of Joint Oceanographic Institutions (JOI), Inc.

References

- Alegret, L., and Thomas, E., 2001. Upper Cretaceous and lower Paleogene benthic foraminifera from northeastern Mexico. *Micropaleontology*, 47(4), 269–316, doi:10.2113/47.4.269.
- Alegret, L., and Thomas, E., 2004. Benthic foraminifera and environmental turnover across the Cretaceous/Paleogene boundary at Blake Nose (ODP Hole 1049C, Northwestern Atlantic). *Palaeogeogr. Palaeoclimatol. Palaeoecol.*, 208, 59–83, doi:10.1016/j.palaeo.2004.02.028.
- Alegret, L., and Thomas, E., 2005. Cretaceous/Paleogene boundary bathyal paleoenvironments in the central North Pacific (DSDP Site 465), the Northwestern Atlantic (ODP Site 1049), the Gulf of Mexico and the Tethys: The benthic foraminiferal record. *Palaeogeogr. Palaeoclimatol. Palaeoecol.*, 224, 53–82, doi:10.1016/j.palaeo.2005.03.031.
- Alegret L., and Thomas E., 2007. Deep-Sea environments across the Cretaceous/Paleogene boundary in the eastern South Atlantic Ocean (ODP Leg 208, Walvis Ridge). *Mar. Micropaleontol.*, 64, 1–17, doi:10.1016/j.marmicro.2006.12.003.
- Alegret, L., and Thomas, E., 2009. Food supply to the seafloor in the Pacific Ocean after the Cretaceous/Paleogene boundary event. *Mar. Micropaleontol.*, 73, 105–116, doi:10.1016/j.marmicro.2009.07.005.

- Alegret, L., and Thomas, E., 2013. Benthic foraminifera across the Cretaceous/Paleogene boundary in the Southern Ocean (ODP Site 690): diversity, food and carbonate saturation. *Mar. Micropaleontol.*, 105, 40-51, doi:10.1016/j.marmicro.2013.10.003.
- Alegret, L., Molina, E., Thomas, E., 2003. Benthic foraminiferal turnover across the Cretaceous/Paleogene boundary at Agost (southeastern Spain): paleoenvironmental inferences. *Mar. Micropaleontol.*, 48, 251-279, doi:10.1016/S0377-8398(03)00022-7.
- Alegret, L., Ortiz, S., Orue-Etxebarria, X., Bernaola, G., Baceta, J.I., Monechi, S., Apellaniz, E., Pujalte, V., 2009a. The Paleocene–Eocene thermal maximum: new data from the microfossil turnover at Zumaia section. *Palaios*, 24, 318–328, <http://dx.doi.org/10.2110/palo.2008.p08-057r>.
- Alegret, L., Ortiz, S., Molina, E., 2009b. Extinction and recovery of benthic foraminifera across the Paleocene–Eocene Thermal Maximum at the Alamedilla section (Southern Spain). *Palaeogeogr. Palaeoclimatol. Palaeoecol.*, 279, 186–200, <http://dx.doi.org/10.1016/j.palaeo.2009.05.009>.
- Alegret, L., Thomas, E., Lohmann, K.C., 2012. End-Cretaceous marine mass extinction not caused by productivity collapse. *Proc. Natl. Acad. Sci. U.S.A.*, 109(3), 728-732, doi:10.1073/pnas.1110601109.
- Alegret, L., Ortiz, S., Arreguín-Rodríguez, G.J., Monechi, S., Millán, I., Molina, E., 2016. Microfossil turnover across the uppermost Danian at Caravaca, Spain: Paleoenvironmental inferences and identification of the latest Danian event. *Palaeogeogr. Palaeoclimatol. Palaeoecol.*, 463, 45-59, doi:10.1016/j.palaeo.2016.09.013.
- Alegret L., Reolid, M., Vega Pérez, M., 2018. Environmental instability during the latest Paleocene at Zumaia (Basque-Cantabric Basin): the bellwether of the Paleocene Eocene Thermal Maximum. *Palaeogeogr. Palaeoclimatol. Palaeoecol.*, 497, 186-200, doi:10.1016/j.palaeo.2018.02.018.

752 Alegret, L., Arreguín-Rodríguez, G. J., Trasviña-Moreno, C. A., Thomas, E., 2021. Turnover and
 753 stability in the deep sea: benthic foraminifera as tracers of Paleogene global change.
 754 Glob. Planet. Change, 196, 103372, doi:10.1016/j.gloplacha.2020.103372.

755 Alvarez, S.A., Gibbs, S.J., Bown, P.R., Kim, H., Sheward, R.M., Ridgwell, A., 2019. Diversity
 756 decoupled from ecosystem function and resilience during mass extinction recovery.
 757 Nature, 574, 242-245, doi:10.1038/s41586-019-1590-8.

758 Arreguín-Rodríguez, G.J. and Alegret, L., 2016. Deep-sea benthic foraminiferal turnover
 759 across early Eocene hyperthermal events at Northeast Atlantic DSDP Site 550.
 760 Palaeogeogr. Palaeoclimatol. Palaeoecol., 451, 62-72,
 761 doi:10.1016/j.palaeo.2016.03.010.

762 Arreguín-Rodríguez, G.J., Alegret, L., Thomas, E., 2016. Late Paleocene – middle Eocene
 763 benthic foraminifera on a Pacific Seamount (Allison Guyot, ODP Site 865):
 764 Greenhouse Climate and superimposed hyperthermal events. Palaeoceanography,
 765 31, 346-364, doi:10.1002/2015PA002837.

766 Arreguín-Rodríguez, G.J., Thomas, E., D'haenens, S., Speijer, R.P., Alegret, L., 2018. Early
 767 Eocene deep-sea benthic foraminiferal faunas: Recovery from the Paleocene Eocene
 768 Thermal Maximum extinction in a greenhouse world. PlosOne, 13(2),
 769 e0193167, <https://doi.org/10.1371/journal.pone.0193167>.

770 Barnet, J.S.K., Littler, K., Kroon, D., Leng, M.J., Westerhold, T., Rohl, U., Zachos, J.C., 2017. A
 771 new high-resolution chronology for the late Maastrichtian warming event:
 772 Establishing robust temporal links with the onset of Deccan volcanism. Geology,
 773 46(2), 147-150, doi:10.1130/G39771.1.

774 Barnet, J.S.K., Littler, K., Westerhold, T., Kroon, D., Leng, M.J., Bailey, I., Röhl, U., Zachos, J.C.,
 775 2019. A high-fidelity benthic stable isotope record of late Cretaceous-early Eocene
 776 climate change and carbon-cycling. Paleoceanogr. Paleoclimatol., 34, 672-691,
 777 doi:10.1029/2019PA003556.

778 Bernaola, G., and Monechi, S., 2007. Calcareous nannofossil extinction and survivorship
 779 across the Cretaceous-Paleogene boundary at Walvis Ridge (ODP Hole 1262C, South
 780 Atlantic Ocean). *Palaeogeogr. Palaeoclimatol. Palaeoecol.*, 255, 132-156,
 781 doi:10.1016/j.palaeo.2007.02.045.

782 Bernaola, G., Baceta, J.I., Orue-Etxebarria, X., Alegret, L., Martín-Rubio, M., Arostegui, J.,
 783 Dinarès-Turell, J., 2007. Evidence of an abrupt environmental disruption during the
 784 mid-Paleocene biotic event (Zumaia section, western Pyrenees). *Geol. Soc. Am. Bull.*,
 785 119(7/8), 785–795, doi:10.1130/B26132.1.

786 Birch, H.S., Coxall, H.K., Pearson, P.N., 2012. Evolutionary ecology of Early Paleocene
 787 planktonic foraminifera: size, depth habitat and symbiosis. *Paleobiology*, 38(3),
 788 374-390, doi:10.1666/11027.1.

789 Birch, H.S., Coxall, H.K., Pearson, P.N., Schmidt, D.N., 2016. Partial collapse of the marine
 790 carbon pump after the Cretaceous-Paleogene boundary. *Geology*, 44(4),
 791 doi:10.1130/G37581.1.

792 Bornemann, A., Schulte, P., Sprong, J., Steurbaut, E., Youssef, M., Speijer, R.P., 2009. Latest
 793 Danian carbon isotope anomaly and associated environmental change in the
 794 southern Tethys (Nile basin, Egypt). *J. Geol. Soc.*, 166, 1135–1142,
 795 doi:10.1144/0016-76492008-104.

796 Boscolo Galazzo, F., Giusberti, L., Luciani, V., Thomas, E., 2013. Paleoenvironmental changes
 797 during the Middle Eocene Climatic Optimum (MECO) and its aftermath: The benthic
 798 foraminiferal record from the Alano section (NE Italy). *Palaeogeogr. Palaeoclimatol.*
 799 *Palaeoecol.*, 378, 22-35, doi:10.1016/j.palaeo.2013.03.018.

800 Boscolo Galazzo, F., Thomas, E., Giusberti, L., 2015. Benthic foraminiferal response to the
 801 Middle Eocene Climatic Optimum (MECO) in the South-Eastern Atlantic (ODP Site
 802 1263). *Palaeogeogr. Palaeoclimatol. Palaeoecol.* 417, 432-444,
 803 doi:10.1016/j.palaeo.2014.10.004.

Bralower, T.J., Premoli Silva, I., Malone, M.J., 2006. Leg 198 synthesis: A remarkable 120-m.y.
 record of climate and oceanography from Shatsky Rise, northwest Pacific Ocean. In:
 Bralower, T.J., Premoli Silva, I., Malone, M.J. (Eds.), *Proceedings of the Ocean Drilling
 Program, Scientific Results*, 198, 1-47.

Bralower, T.J., Cosmidis, J. Heaney, P.J., Kump, L.R., Morgan, J.V., Harper, D.T., Lyons, S.L.,
 Freeman, K.H., Grice, K., Wendler, J.E., Zachos, J.C., Artemieva, N., Si. A.C., Gulick, S.P.S.,
 House, C.H., Jones, H.L., Lowery, C.M., Nims, C., Schaefer, B., Thomas, E., Vajda, V.,
 2020. Origin of a global carbonate layer deposited in the aftermath of the
 Cretaceous-Paleogene boundary impact. *Earth Planet. Sci. Lett.*, 548, 115476;
 doi:10.1016/j.epsl.2020.116476.

Coccioni, R., Frontalini, F., Bancalà, G., Fornaciari, E., Jovane, L., Sprovieri, M., 2010. The Dan-
 C2 hyperthermal event at Gubio (Italy): Global implications, environmental effects,
 and cause(s). *Earth Planet. Sci. Lett.*, 297, 298–305, doi:10.1016/j.epsl.2010.06.031.

Cramer, B.S., Wright, J.D., Kent, D.V., Aubry, M.P., 2003. Orbital climate forcing of $\delta^{13}\text{C}$ ex-
 cursions in the late Paleocene–early Eocene (chrons C24n–C25n).
Paleoceanography, 18(4), 1097, <http://dx.doi.org/10.1029/2003PA000909>.

DeConto, R.M., Galeotti, S., Pagani, M., Tracy, D., Schaefer, K., Zhang, T., Pollard, D., Beerling,
 D.J., 2012. Past extreme warming events linked to massive carbon release from
 thawing permafrost. *Nature*, 484(7392), 87–91,
<https://doi.org/10.1038/nature10929>.

Deprez, A., Tesseur, S., Stassen, P., D’haenens, S., Steurbaut, E., King, C., Claeys, P., Speijer,
 R.P., 2015. Early Eocene environmental development in the northern Peri-Tethys
 (Aktulagay, Kazakhstan) based on benthic foraminiferal assemblages and stable
 isotopes (O, C). *Mar. Micropaleontol.*, 115, 59–71,
 doi:10.1016/j.marmicro.2014.11.003.

829 Deprez, A., Jehle, S., Bornemann, A., Speijer, R.P., 2017. Differential response at the seafloor
830 during Paleocene and Eocene ocean warming events at Walvis Ridge, Atlantic Ocean
831 (ODP Site 1262). *Terra Nova*, 29, 71-76, doi:10.1111/ter.12250.

832 D'haenens, S., Bornemann, A., Stassen, P., Speijer, R.P., 2012. Multiple early Eocene benthic
833 foraminiferal assemblage and $\delta^{13}\text{C}$ fluctuations at DSDP Site 401 (Bay of Biscay—
834 NE Atlantic). *Mar. Micropaleontol.*, 88–89, 15–35, doi:10.1016/j.marmicro.
835 2012.02.006.

836 D'Hondt, S., 2005. Consequences of the Cretaceous/Paleogene mass extinction for the
837 marine ecosystems. *Annu. Rev. Ecol. Evol. Syst.*, 36, 295–317,
838 doi:10.1146/annurev.ecolsys.35.021103.105715.

839 Dickens, G.R., 2011. Down the Rabbit Hole: toward appropriate discussion of methane
840 release from gas hydrate systems during the Paleocene-Eocene thermal maximum
841 and other past hyperthermal events. *Clim. Past*, 7, 831–846.

842 Dinarès-Turell, J., Westerhold, T., Pujalte, V., Röhl, U., Kroon, D., 2014. Astronomical
843 calibration of the Danian stage (Early Paleocene) revisited: Settling chronologies of
844 sedimentary records across the Atlantic and Pacific Oceans. *Earth Planet. Sci. Lett.*,
845 405, 119–131, doi:10.1016/j.epsl.2014.08.027.

846 Esmeray-Senlet, S., Wright, J.D., Olsson, R.K., Miller, K.G., Browning, J.V., Quan, T.M., 2015.
847 Evidence for reduced export productivity following the Cretaceous/Paleogene mass
848 extinction. *Paleoceanography*, 30, 718–738, doi:10.1002/2014PA002724.

849 Fenero, R., Thomas, E., Alegret, L., Molina, E., 2012. Oligocene benthic foraminifera from the
850 Fuente Caldera section (Spain, western Tethys): taxonomy and paleoenvironmental
851 inferences. *J. Foraminifer. Res.*, 42, 286–304.

852 Fligner, M.A., and Killeen, T.J., 1976. Distribution-free two sample tests for scale. *J. Am. Stat.*
853 *Assoc.*, 71, 210–213.

854 Fontanier, C., Jorissen, F.J., Licari, L., Alexandre, A., Anschutz, P., Carbonel, P., 2002. Live
855 benthic foraminiferal faunas from the Bay of Biscay: faunal density, composition and

856 microhabitats. Deep-Sea Res. I, 49, 751–785, doi:10.1016/S0967-0637(01)00078-
857 4.

858 Friedrich, O., and Hemleben, C., 2007. Early Maastrichtian benthic foraminiferal
859 assemblages from the western North Atlantic (Blake Nose) and their relation to
860 paleoenvironmental changes. Mar. Micropaleontol., 62, 31-44,
861 doi:10.1016/j.marmicro.2006.07.003.

862 Galeotti, S., Moretti, M., Cappelli, C., Phillips, J., Lanci, L., Littler, K., Monechi, S., Petrizzo, M.
863 R., Premoli-Silva, I., Zachos, J. C., 2015. The Bottaccione section at Gubbio, central
864 Italy: a classical Paleocene Tethyan setting revisited. Newsl. Stratigr., 48, 325-339.

865 Gibbs, S.J., Bown, P.R., Ward, B.A., Alvarez, S.A., Kim, H., Archontikis, O.A., Sauterey, B.,
866 Poulton, A.J., Wilson, J., Ridgwell, A., 2020. Algal plankton turn to hunting to survive
867 and recover from end-Cretaceous impact darkness. Sci. Adv., 6, eabc9123,
868 doi:10.1126/sciadv.abc9123.

869 Gilmour, I., Gilmour, M., Jolley, D., Kelley, S., Kemp, D., Daly, R., Watson, J., 2013. A high-
870 resolution nonmarine record of an early Danian hyperthermal event, Boltysh crater,
871 Ukraine. Geology, 41(7), 783–786, doi:10.1130/G34292.1.

872 Gooday, A.J., 2003. Benthic foraminifera (Protista) as tools in deep-water
873 palaeoceanography: Environmental influences on faunal characteristics. Advances
874 in Marine Biology, 46, 1–90.

875 Gradstein, F.M., Ogg, J.G., Smith, A.G., 2004. A geological time scale 2004. Cambridge
876 University Press, Cambridge, UK.

877 Griffith, E.M., Thomas, E., Lewis, A.R., Penman, D.E., Westerhold, T., Winguth, A.M.E., 2021.
878 Benthic-pelagic Decoupling: The Marine Biological Carbon Pump During Eocene
879 Hyperthermals. Paleoclimatol., 36, e2020PA004053.

880 Hammer, Ø., Harper, D.A.T., Ryan, P.D., 2001. PAST: Paleontological Statistics Software
881 Package for Education and Data Analysis. Palaeontol. Electron., 4(1), 1–9.

882 Hay, W., de Conto, R.M., Wold, C.N., Wilson, K.M., Voigt, S., Schulz, M., Wold, A.R., Dullo, W.C.,
883 Ronov, A.B., Balukhovsky, A.N., Söding, E., 1999. Alternative global Cretaceous
884 paleogeography. In: Barrera, E., Jonhson, C.C. (Eds.), *Evolution of the Cretaceous*
885 *Ocean–Climate System 332*, Geological Society of America Special Paper, 1–47.

886 Hayek, L.-A., Buzas, M., Thomas, E., 2019. Identifying disruptions to the ecological balance
887 of nature: a foraminiferal example across the initiation of the Paleocene-Eocene
888 Thermal Maximum. *Paleobiology*, 45, 98-113.

889 Hayward, B.W., Kawata, S., Sabaa, A., Grenfell, H., Van Kerckhoven, L., Johnson, K., Thomas,
890 E., 2012. The last global extinction (Mid-Pleistocene) of deep-sea benthic
891 foraminifera (Chrysalogoniidae, Ellipsoidinidae, Glandulonodosariidae,
892 Plectofrondiculariidae, Pleurostomellidae, Stilostomellidae), Their Late
893 Cretaceous–Cenozoic history and taxonomy. *Cushman Foundation for Foraminiferal*
894 *Research Special Publications 43*, Allen Press, USA.

895 Henehan, M.J., Ridgwell, A., Thomas, E., Zhang, S., Alegret, L., Schmidt, D.N., Rae, J.W.B., Witts,
896 J.D., Landman, N.H., Greene, S.E., Huber, B.T., Super, J., Planavsky, N.J., Hull, P.M.,
897 2019. Rapid ocean acidification and protracted Earth System recovery followed the
898 end-Cretaceous Chicxulub impact. *Proc. Natl. Acad. Sci. U.S.A.*, 116, 22500-22504,
899 doi:10.1073/pnas.1905989116.

900 Herguera, J.C., and Berger, W., 1991. Paleoproductivity from benthonic foraminifera
901 abundance: Glacial to postglacial change in the west-equatorial Pacific. *Geology*, 19,
902 1173–1176.

903 Hull, P.M., and Norris, R.D., 2011. Diverse patterns of ocean export productivity change
904 across the Cretaceous-Paleogene boundary: New insights from biogenic barium.
905 *Paleoceanography* 26, PA3205.

906 Hull, P.M., Bornemann, A., Penman, D.E., Henehan, M.J., Norris, R.D., Wilson, P.A., Blum, P.,
907 Alegret, L., Batenburg, S.J., Bown, P.R., Bralower, T.J., Cournede, C., Deutsch, A.,
908 Donner, B., Friedrich, O., Jehle, S., Kim, H., Kroon, D., Lippert, P.C., Lorocho, D., Moebius,

909 I., Moriya, K., Peppe, D.J., Ravizza, G.E., Röhl, U., Schueth, J.D., Sepulveda, J., Sexton,
 910 P.F., Sibert, E.C., Sliwinska, K.K., Summons, R.E., Thomas, E., Westerhold, T.,
 911 Whiteside, J.H., Yamaguchi, T., Zachos, J.C., 2020. On impact and volcanism across the
 912 Cretaceous-Paleogene boundary. *Science*, 367, 266-
 913 272, doi:10.1126/science.aay5055.

914 Jennions, S.M., Thomas, E., Schmidt, D.N., Lunt, D., Ridgwell, A., 2015. Changes in benthic
 915 ecosystems and ocean circulation in the Southeast Atlantic across Eocene Thermal
 916 Maximum 2. *Paleoceanography*, 30, 1059-1077, doi:10.1002/2015PA002821.

917 Jorissen, F.J., De Stigter, H.C., Widmark, J.G.V., 1995. A conceptual model explaining benthic
 918 foraminiferal microhabitats. *Mar. Micropaleontol.*, 26, 3–15.

919 Jorissen, F.J., Fontanier, C., Thomas, E., 2007. Paleoceanographical proxies based on deep-
 920 sea benthic foraminiferal assemblage characteristics. In: Hillaire-Marcel, C., and de
 921 Vernal, A. (Eds.), *Developments in Marine Geology: Proxies in Late Cenozoic*
 922 *Paleoceanography: Pt. 2: Biological tracers and biomarkers*. Elsevier, Amsterdam,
 923 263–326, doi:10.1016/S1572-5480(07)01012-3.

924 Kaminski, M. A., and Gradstein, F. M., 2005. *Atlas of Paleogene cosmopolitan deep-water*
 925 *agglutinated foraminifera*. Grzybowski Foundation, Special Publication, 10, 547 pp.

926 Katz, M.E., and Miller, K.G., 1991. Early Paleogene benthic foraminiferal assemblages and
 927 stable isotopes in the Southern Ocean. *Proceedings of the Ocean Drilling Program*
 928 *Scientific Reports* 114, 481–512.

929 Kroon, D., Zachos, J.C., et al., 2007. 1. Leg 208 Synthesis: Cenozoic climate cycles and
 930 excursions. In: Kroon, D., Zachos, J.C., Richter, C. (Eds.), *Proceedings of the Ocean*
 931 *Drilling Program, Scientific Results* 208, 1-55.

932 Leon-Rodriguez, L., and Dickens, G.R., 2010. Constraints on ocean acidification associated
 933 with rapid and massive carbon injections: the early Paleogene record at ocean
 934 drilling program site 1215, equatorial Pacific Ocean. *Palaeogeogr. Palaeoclimatol.*
 935 *Palaeoecol.*, 298, 409–420, doi:10.1016/j.palaeo.2010.10.029.

936 Littler, K., Röhl, U., Westerhold, T., Zachos, J.C., 2014. A high-resolution benthic stable-
 937 isotope record for the South Atlantic: implications for orbital-scale changes in Late
 938 Paleocene–Early Eocene climate and carbon cycling. *Earth Planet. Sci. Lett.*, 401, 18–
 939 30, doi:10.1016/j.epsl.2014.05.054.

940 Loeblich Jr., A.R., and Tappan, H., 1988. *Foraminifera Genera and Their Classification*. Van
 941 Nostrand Reinhold Company Inc., New York.

942 Lourens, L., Sluijs, A., Kroon, D., Zachos, J.C., Thomas, E., Roehl, U., Bowles, J., Raffi, I., 2005.
 943 Astronomical modulation of late Palaeocene to early Eocene global warming events.
 944 *Nature*, 435, 1083–1087, doi:10.1038/nature0381.

945 Lowery, C.M., Bralower, T.J., Owens, J.D., Rodríguez-Tovar, F.J., Jones, H., Smith, J., Whalen,
 946 M.T., Claeys, P., Farley, K., Gulick, S.P.S., Morgan, J.V., Green, S., Chenot, E., Christeson,
 947 G.L., Cockell, C.S., Coolen, M.J.L., Ferrière, L., Gebhardt, C., Goto, K., Kring, D.A., Lofi, J.,
 948 Ocampo-Torres, R., Perez-Cruz, L., Pickersgill, A.E., Poelchau, M.H., Rae, A.S.P.,
 949 Rassmussen, C., Rebolledo-Vieyra, M., Riller, U., Sato, H., Tikoo, S.M., Tomioka, N.,
 950 Urrutia-Fucugauchi, J., Vellekoop, J., Wittmann, A., Xiao, L., Yamaguchi, K.E.,
 951 Zylberman, W., 2018. Rapid recovery of life at ground zero of the end-Cretaceous
 952 mass extinction. *Nature*, 558, 288–291, doi:10.1038/s41586-018-0163-6.

953 McInerney, F.A., and Wing, S., 2011. The Paleocene–Eocene Thermal Maximum: a
 954 perturbation of carbon cycle, climate, and biosphere with implications for the future.
 955 *Annu. Rev. Earth Planet. Sci.*, 39, 489–516, doi:10.1146/annurev-earth-040610-
 956 133431.

957 Mello, R.M., Leckie, R.M., Fraass, A.J., Thomas, E., 2017. Upper Maastrichtian – Eocene
 958 benthic foraminiferal biofacies of the Brazilian margin, western South Atlantic. In:
 959 Kaminski, M.A., Alegret, L., (Eds), *Proceedings of the 9th International Workshop on*
 960 *Agglutinated Foraminifera*, Grzybowski Foundation Special Publication, 22: 119–
 961 161.

962 Miller, K.G., Janecek, T.R., Katz, M.E., Keil, D.J., 1987. Abyssal circulation and benthic
 963 foraminiferal changes near the Paleocene/Eocene boundary. *Paleoceanography*, 2,
 964 741–761.

965 Minoletti F, de Rafaelis M, Renard M, Gardin S, Young J., 2005. Changes in the pelagic fine
 966 fraction carbonate sedimentation during the Cretaceous-Paleocene transition:
 967 Contribution of the separation technique to the study of the Bidart section.
 968 *Palaeogeogr., Palaeoclimatol., Palaeoecol.*, 216, 119–137.

969 Petrizzo, M.R., 2005. An early late Paleocene event on Shatsky Rise, northwest Pacific Ocean
 970 (ODP Leg 198), Evidence from planktonic foraminiferal assemblages. *Proceedings*
 971 *of the Ocean Drilling Program Scientific Results* 198, 1-29,
 972 doi:10.2973/odp.proc.sr.198.102.2005.

973 Quillévéré, F., Norris, R.D., Kroon, D., Wilson, P.A., 2008. Transient ocean warming and shifts
 974 in carbon reservoirs during the early Danian. *Earth Planet. Sci. Lett.*, 265, 600–615,
 975 doi:10.1016/j.epsl.2007.10.040.

976 Ridgwell, A.J., 2005. A mid Mesozoic revolution in the regulation of ocean chemistry. *Mar.*
 977 *Geol.*, 217, 339-357.

978 Ridgwell, A.J., and Zeebe, R.E., 2005. The role of the global carbonate cycle in the regulation
 979 and evolution of the Earth system. *Earth Planet. Sci. Lett.*, 234, 299-315,
 980 doi:10.1016/j.epsl.2005.03.006.

981 Schaefer, B., Grice, K., Coolen, M.J.L., Summons, R.E., Cui, X., Bauersachs, T., Schwark, L.,
 982 Böttcher, M.E., Bralower, T.J., Lyons, S.L., Freeman, K.H., Cockell, C.S., Gulick, S.P.S.,
 983 Morgan, J.V., Whalen, M.T., Lowery, C.M., Vajda, V., 2020. Microbial life in the nascent
 984 Chicxulub crater. *Geology*, 48, 328-332, doi:10.1130/G46799.1.

985 Schueth, J.D., Bralower, T.J., Jiang, S., Patzkowsky, M.E., 2015. The role of regional survivor
 986 incumbency in the evolutionary recovery of calcareous nannoplankton from the
 987 Cretaceous/Paleogene (K/Pg) mass extinction. *Paleobiology*, 41, 661–
 988 679, doi:10.1017/pab.2015.28.

989 Sen Gupta, B.K., and Machain-Castillo, M.L., 1993. Benthic foraminifera in oxygen-poor
 990 habitats. *Mar. Micropaleontol.*, 20, 3–4.

991 Sepulveda, J., Wendler, J.E., Summons, R.E., Hinrichs, K.U., 2009. Rapid resurgence of marine
 992 productivity after the Cretaceous-Paleogene mass extinction. *Science*, 326, 129-132,
 993 doi:10.1126/science.1176233.

994 Sepulveda, J., Alegret, L., Thomas, E., Haddad, E., Cao, C., Summons, R.E., 2019. Stable isotope
 995 constraints on marine productivity across the Cretaceous-Paleogene mass
 996 extinction. *Paleoceanogr. Paleoclimatol.*, 34, 1195-1217,
 997 doi:10.1029/2018PA003442.

998 Speed, C.D., and Kroon, D., 2000. Data report: inorganic geochemistry and mineralogy of the
 999 Cretaceous/Tertiary Boundary in hole 1049C. In: Kroon, D., Norris, R.D., Klaus, A.
 1000 (Eds.), *Proceedings of the Ocean Drilling Program, Scientific Results, 171B, Ocean*
 1001 *Drilling Program, Texas A and M University* 1–26.

1002 Speijer, R.P., Scheibner, C., Stassen, P., Morsi, A.-M., 2012. Response of marine ecosystems to
 1003 deep-time global warming: a synthesis of biotic patterns across the Paleocene-
 1004 Eocene thermal maximum (PETM). *Austrian J. Earth Sci.*, 105, 6–16.

1005 Sprong, J., Kouwenhoven, T.J., Bornemann, A., Dupuis, C., Speijer, R.P., Stassen, P., Steurbaut,
 1006 E., 2013. In search of the Latest Danian Event in a paleobathymetric transect off
 1007 Kasserine Island, north-central Tunisia. *Palaeogeogr. Palaeoclimatol. Palaeoecol.*,
 1008 379-380, 1-16, doi:10.1016/j.palaeo.2013.01.018.

1009 Stap, L., Sluijs, A., Thomas, E., Lourens, L., 2009. Patterns and magnitude of deep sea
 1010 carbonate dissolution during Eocene Thermal Maximum 2 and H2, Walvis Ridge,
 1011 South-Eastern Atlantic Ocean. *Paleoceanography*, 24, PA1211,
 1012 doi:10.1029/2008PA001655.

1013 Stap, L., Lourens, L.J., Thomas, E., Sluijs, A., Bohaty, S., Zachos, J.C., 2010. High-resolution
 1014 deep-sea carbon and oxygen isotope records of Eocene Thermal Maximum 2 and H2.
 1015 *Geology*, 38, 607–610, doi:10.1130/G30777.1.

1016 Thomas, E., 1989. Development of Cenozoic deep-sea benthic foraminiferal faunas in
1017 Antarctic waters. In: Crame, J.A. (Ed.), *Origins and evolution of Antarctic biota*,
1018 Geological Society Special Publication 47, 283-296.

1019 Thomas, E., 1990a. Late Cretaceous–early Eocene mass extinctions in the deep sea. In:
1020 Sharpton, V.L., Ward, P.D. (Eds.), *Global Catastrophes in Earth History: An*
1021 *Interdisciplinary Conference on Impacts, Volcanism, and Mass Mortality*. Geological
1022 Society of America, Special Paper Vol. 247, 481–495.

1023 Thomas, E., 1990b. Late Cretaceous through Neogene deep-sea benthic foraminifers (Maud
1024 Rise, Weddell Sea, Antarctica). In: Barker, P.F., Kennett, J.P., et al. (Eds.), *Proceedings*
1025 *of the Ocean Drilling Program, Scientific results, Volume 113: College Station, Texas,*
1026 *Ocean Drilling Program*, 571–594.

1027 Thomas, E., 1998. The biogeography of the late Paleocene benthic foraminiferal extinction.
1028 In: Aubry, M.P., Lucas, S., Berggren, W.A. (Eds.), *Late Paleocene–Early Eocene Biotic*
1029 *and Climatic Events in the Marine and Terrestrial Records*. Columbia University
1030 Press, New York, 214–243.

1031 Thomas, E., 2003. Extinction and food at the seafloor: A high-resolution benthic
1032 foraminiferal record across the Initial Eocene Thermal Maximum, Southern Ocean
1033 Site 690. In: Wing, S.L., Gingerich, P.D., Schmitz, B., and Thomas, E. (Eds.), *Causes and*
1034 *Consequences of Globally Warm Climates in the Early Paleogene*. Geological Society
1035 of America, Special Paper, 369, 319–332.

1036 Thomas, E., 2007. Cenozoic mass extinctions in the deep sea; what disturbs the largest
1037 habitat on Earth? In: Monechi, S., Coccioni, R., Rampino, M. (Eds.), *Large Ecosystem*
1038 *Perturbations: Causes and Consequences*, Special Paper 424. Geological Society of
1039 America, Boulder, Colorado, 1–24, doi:10.1130/2007.2424(01).

1040 Thomas, E., and Zachos, J.C., 2000. Was the late Paleocene thermal maximum a unique
1041 event? *Geol. Foeren. Stockholm Foerh.*, 122, 169–170.

1042 Thomas, E., Zachos, J.C., Bralower, T.J., 2000. Deep-sea environments on a warm Earth: latest
1043 Paleocene–early Eocene. In: Huber, B., et al. (Eds.), *Warm Climates in Earth History*.
1044 Cambridge University Press, UK, 132–160.

1045 Thomas, E., Schmidt, D., Kroon, D., Alegret, L., Bernaola, G., Lohmann, K.C., Monechi, S., Röhl,
1046 U., Westerhold, T., 2007. Effects of the end Cretaceous asteroid impact, Walvis Ridge,
1047 SE Atlantic Ocean. ICP9, Shanghai, China, September 3-7, 2007. ICP9, Shanghai,
1048 China, September 3-7, 2007, p. 96.

1049 Thomas, E., Boscolo-Galazzo, F., Balestra, B., Monechi, S., Donner, B., Röhl, U., 2018. Early
1050 Eocene Thermal Maximum 3: Biotic response at Walvis Ridge (SE Atlantic Ocean).
1051 *Paleoceanogr. Paleoclimatol.*, 33, 8, 862-883, doi:10.1029/2018PA003375.

1052 Tjalsma, R.C., and Lohmann, G.P., 1983. Paleocene–Eocene bathyal and abyssal benthic
1053 foraminifera from the Atlantic Ocean. *Micropaleontology Special Publication*, 4, 1–
1054 89.

1055 Van Morkhoven, F.P.C.M., Berggren, W.A., Edwards, A.S., 1986. Cenozoic cosmopolitan deep-
1056 water benthic foraminifera. *Bulletin des Centres de Recherche Exploration —*
1057 *Production Elf-Aquitaine Memoir Vol. 11*. Pau, France.

1058 Westerhold, T., Röhl, U., Raffi, I., Fornaciari, E., Monechi, S., Reale, V., Bowles, J., Evans, H.F.,
1059 2008. Astronomical calibration of the Paleocene time. *Palaeogeogr. Palaeoclimatol.*
1060 *Palaeoecol.*, 257, 377–403, doi:10.1016/j.palaeo.2007.09.016.

1061 Westerhold, T., Röhl, U., Donner, B., McCarren, H.K., Zachos, J.C., 2011. A complete high-
1062 resolution Paleocene benthic stable isotope record for the Central Pacific (ODP site
1063 1209). *Paleoceanography*, 26, PA2216, doi:10.1029/2010PA002092.

1064 Westerhold, T., Röhl, U., Frederichs, T., Agnini, C., Raffi, I., Zachos, J.C., Wilkens, R.H., 2017.
1065 Astronomical calibration of the Ypresian timescale: implications for seafloor
1066 spreading rates and the chaotic behavior of the solar system? *Clim. Past*, 13, 1129-
1067 1152, doi:10.5194/cp-2017-15.

- Westerhold, T., Röhl, U., Wilkens, R.H., Gingerich, P.D., Clyde, W.C., Wing, S.L., Bowen, G.J., Kraus, M.J., 2018. Synchronizing early Eocene deep-sea and continental records – cyclostratigraphic age models for the Bighorn Basin Coring Project drill cores. *Clim. Past*, 14, 393-319, doi:10.5194/cp-14-303-2018.
- Westerhold, T., Marwan, N., Drury, A.J., Liebrand, D., Agnini, C., Anagnostou, E., Barnet, J.S.K., Bohaty, S.M., De Vleeschouwer, D., Florindo, F., Frederichs, T., Hodell, D.A., Holbourn, A.E., Kroon, D., Lauretano, V., Littler, K., Lourens, L.J., Lyle, M., Pälike, H., Röhl, U., Tian, J., Wilkens, R.H., Wilson, P.A., Zachos, J.C., 2020. An astronomically dated record of Earth's climate and its predictability over the last 66 million years. *Science*, 369, 1383-1387, doi:10.1126/science.aba6853.
- Widmark, J.G.V., and Malmgren, B., 1992. Benthic foraminiferal changes across the Cretaceous-Tertiary boundary in the deep sea: DSDP Sites 525, 527 and 465. *J. Foraminifer. Res.*, 22, 81-113.
- Zachos, J.C., Kroon, D., Blum, P., et al., 2004. Site 1262. In: Zachos, J.C., Kroon, D., Blum, P., et al. (Eds.), *Proceedings of the Ocean Drilling Program, Initial Reports 208*. Ocean Drilling Program, College Station, TX, 1–92, doi:10.2973/odp.proc.ir.208.103.2004.
- Zeebe, R.E., and Lourens, L.J., 2019. Solar System chaos and the Paleocene–Eocene boundary age constrained by geology and astronomy. *Science* 365, 926-929, doi:10.1126/science.aax0612.
- Zeebe, R.E., and Westbroek, P., 2003. A simple model for the CaCO₃ saturation state of the ocean: The “Strangelove,” the “Neritan,” and the “Cretan” Ocean. *Geochem. Geophys. Geosyst.*, 4(12), 1104, doi:10.1029/2003GC000538.

Supplementary material captions:

Figure S1. Correlation plots and regression lines between %CaCO₃ (Alegret et al., 2012) and distinct variables: relative abundance of agglutinated taxa (a), diversity index (b),

1095 heterogeneity index (c), as well as percentages of polymorphinids (d), unilocular taxa (e),
1096 uniserial lagenids (f), and stilostomellids (g).

1097

1098 Table S1. Quantitative data of benthic foraminifera and MAR_{bulk} data from ODP Site 1262.

1099

1100 Table S2. Taxonomic list and original references of common benthic foraminiferal species
1101 at ODP Site 1262 in the lower Paleocene.